Contrib Mineral Petrol (2008) 156:477–500
DOI 10.1007/s00410-008-0297-x

ORIGINAL PAPER

Petrogenesis of Permian alkaline lamprophyres and diabases from the Spanish Central System and their geodynamic context within western Europe

D. Orejana · C. Villaseca · K. Billström · B. A. Paterson

Received: 6 September 2007 / Accepted: 12 March 2008 / Published online: 1 April 2008

Abstract Basic to ultrabasic alkaline lamprophyres and diabases intruded within the Spanish Central System (SCS) during Upper Permian. Their high LREE, LILE and HFSE contents, together with positive Nb–Ta anomalies, link their origin with the infiltration of sublithospheric K-rich fluids. These alkaline dykes may be classified in two distinct groups according to the Sr–Nd isotope ratios: (1) a depleted PREMA-like asthenospheric component, and (2) a BSE-like lithospheric component. A slight enrichment in radiogenic ^{207}Pb and ^{208}Pb allows the contribution of a recycled crustal or lithospheric component in the mantle sources. The intrusion of this alkaline magmatism is likely to have occurred due to adiabatic decompression and mantle upwelling in the context of the widespread rifting developed from Carboniferous to Permian in western Europe. The clear differences in the geochemical affinity of Lower Permian basic magmas from north-western and south-western Europe might be interpreted in terms of a more extensive separation of both regions during that period, until they were assembled during Upper Permian.

Communicated by J. Hoefs.

Electronic supplementary material The online version of this article (doi:10.1007/s00410-008-0297-x) contains supplementary material, which is available to authorized users.

D. Orejana (✉) · C. Villaseca
Department of Petrology and Geochemistry,
Complutense University of Madrid, 28040 Madrid, Spain
e-mail: dorejana@geo.ucm.es

K. Billström
Museum of Natural History, Stockholm, Sweden

B. A. Paterson
Department of Earth Sciences, University of Bristol,
BS8 1RJ Bristol, UK

Keywords Lamprophyres · Alkaline magmatism · Asthenospheric mantle · Permian rifting · Western Europe

Introduction

Alkaline lamprophyres are considered to be the equivalent of basaltic rocks with high volatile contents, being related to partial melting of a hydrated mantle enriched in incompatible elements (Rock 1991). The incorporation of volatiles is thought to be due to metasomatism by infiltrating fluids or silicate melts ascending from lithospheric or sub-lithospheric sources (e.g. Hawkesworth et al. 1990).

Mafic alkaline lamprophyres were intruded during the Upper Permian in the Spanish Central System (SCS). Other moderately alkaline rocks from the Iberian Peninsula are broadly coeval with these lamprophyres (mafic dykes from Pyrenees; Debon and Zimmermann 1993), or are very similar in age (North Portugal; Portugal-Ferreira and Macedo 1977), though their exact geochronology has yet to be constrained. In any case, this intraplate magmatism represents a small volume of intruded magma. Previous studies, which focused on the Permo-Carboniferous magmatism from central Spain (Perini et al. 2004) and on the Hercynian and post-Hercynian basic rocks of the SCS (Bea et al. 1999), have advocated a lithospheric origin for the mantle sources of the SCS alkaline lamprophyres. Other studies have revealed that part of the SCS Permian alkaline basic intrusions show an isotopically depleted component, indicative of greater heterogeneity than previously suggested and the involvement of sub-lithospheric sources (Villaseca et al. 2004; Orejana et al. 2005).

The geodynamic setting proposed for these dyke swarms is also the subject of debate. Some authors link their generation to manifestations of Permo-Carboniferous

magmatism related to the impingement of a mantle plume prior to the opening of the Atlantic Ocean (Doblas et al. 1998; Perini et al. 2004), whereas others consider that rifting in this region could result from lithosphere thinning and adiabatic upwelling of the hot asphenosphere (Orejana et al. 2006).

In this study we present new data, including major and trace element mineral analyses, bulk-rock composition and isotope ratios (Sr–Nd–Pb), which allow us to elucidate the petrogenesis of these alkaline dykes. The new sample set covers the whole outcropping region of every dyke swarm, and considerably enlarging the previously available analytical dataset. Particular emphasis is placed on the heterogeneity of the mantle sources, the possible role of crustal components and on the nature of any metasomatising agents. Furthermore, we also discuss the significance of the geochemical differences that exist in the widespread Permian basic magmatism developed at the end of the Hercynian orogeny in north-western and south-western Europe.

Geological setting

The SCS is located within the Central-Iberian Zone of the Iberian Massif (Fig. 1). This is a large batholith that consists of several granitic bodies emplaced into Palaeozoic to Neoproterozoic orthogneisses and metasediments. The first manifestation of this granite magmatism has been dated at 346 ± 63 Ma (Villaseca et al. 1998a), approximately 50 Ma after the beginning of the Hercynian collision (408–387 Ma; Gutiérrez Marco et al. 1990). In volume terms the most important plutons were emplaced in the range 323–284 Ma (Villaseca et al. 1998b; Bea et al. 1999; Zeck et al. 2007). The SCS Hercynian granitoids are mainly peraluminous felsic varieties displaying a narrow compositional range, and which do not show any marked compositional trend with time (Villaseca and Herreros 2000).

Hercynian basic intrusions in the SCS are volumetrically small and occur as small gabbroic to quartz-dioritic masses. Ages range from 322 ± 5 Ma (Rb–Sr whole-rock isochron; Casillas et al. 1991) to 306 ± 2 Ma (SIMS U–Pb dating of zircon; Zeck et al. 2007). Based on their geochemistry these rocks have been linked to crustal recycling in the mantle or melting of a subduction-modified mantle source (Villaseca et al. 2004). In addition to these minor basic intrusives, the SCS is cross-cut by a number of different post-collisional dyke swarms (Fig. 1): (1) E-W oriented calc-alkaline microdiorites (290 ± 10 Ma, Rb–Sr

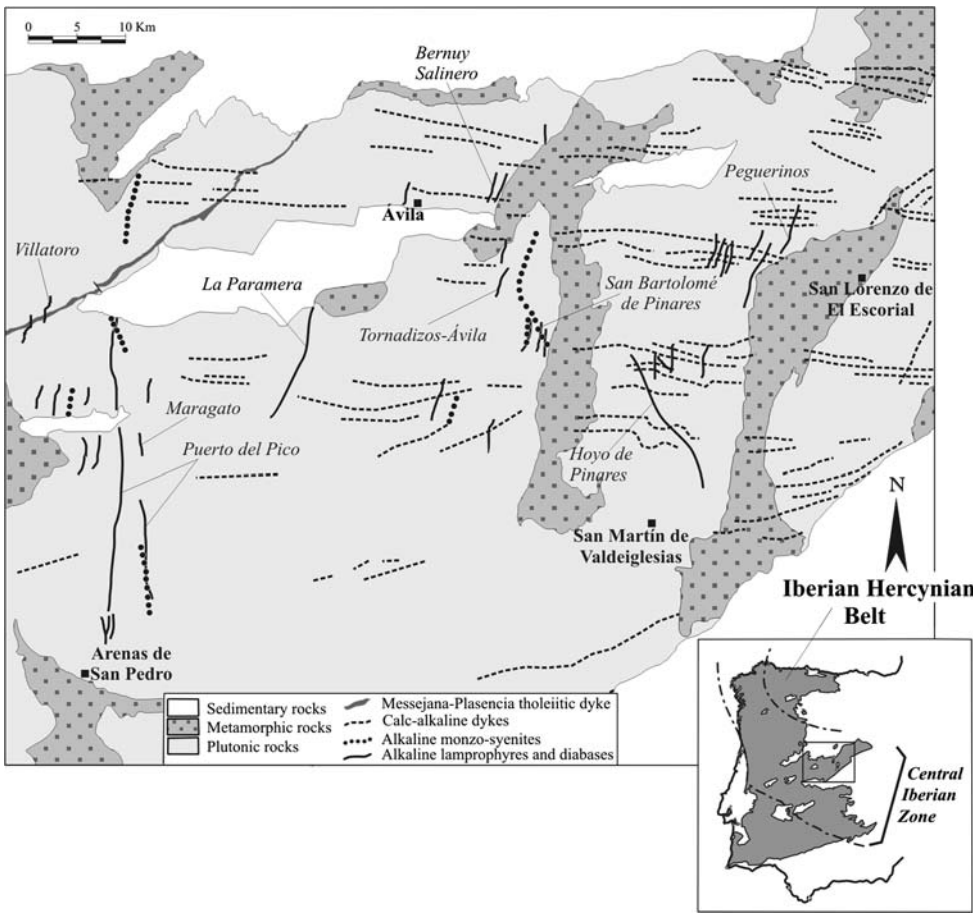

Fig. 1 Schematic map showing the Permian alkaline lamprophyres and diabases from the SCS, together with other post-collisional magmatic intrusions of calc-alkaline and tholeiitic affinity. The names of the nine dyke swarms sampled in this study are indicated in *italics*

isochron; Galindo et al. 1994), (2) shoshonitic microgabbros, and (3) N-S oriented alkaline dykes. The first two sets are associated with coeval granite porphyries. These three dyke swarm sets have been classified by Villaseca et al. (2004) into the following groupings, Gb2, Gb3 and Gb4, respectively. The Gb1 group was assigned to the previously mentioned Hercynian gabbroic to quartz-dioritic masses. The last magmatic event recorded in the SCS is represented by the intrusion of the large gabbroic Messejana–Plasencia tholeiitic dyke (named Gb5 by Villaseca et al. 2004), dated at 203 ± 2 Ma (Ar–Ar in biotite; Dunn et al. 1998), which is linked to the opening of the Atlantic Ocean.

The alkaline suite (Gb4 group) may be further subdivided into: (1) basic to ultrabasic lamprophyres and diabases, and (2) monzogabbroic to syenitic porphyries. The most recent geochronological data obtained for these rocks give Upper Permian intrusive ages between 264 ± 1 Ma (Ar–Ar on amphibole from lamprophyre dykes; Perini et al. 2004; Scarrow et al. 2006) and 252 ± 3 Ma (U–Pb on zircon from a syenitic porphyry; Fernández Suárez et al. 2006). The lamprophyres carry xenocrysts and megacrysts (mainly clinopyroxene, amphibole and plagioclase), and also xenoliths that are relatively abundant in some outcrops. The latter can be broadly subdivided into granulite and ultramafic xenoliths. Most of the SCS granulites have been interpreted as lower crustal restites formed as the result of extraction of the granite melts which led to the formation of the SCS batholith (Villaseca et al. 1999). Mafic to ultramafic xenoliths, on the contrary, are deep pyroxenitic cumulates that crystallised directly from Permian alkaline basic magmas or melts related to Hercynian calc-alkaline mafic underplating events (Orejana et al. 2006).

Analytical methods

The major element composition of minerals from SCS alkaline lamprophyres and diabases were determined at the *Centro de Microscopía Electrónica "Luis Bru"* (*Complutentse University of Madrid*) using a Jeol JZA-8900 M electron microprobe with four wavelength dispersive spectrometers. Accelerating voltage was 15 kV and the electron beam current 20 nA, with a beam diameter of 5 μm. Elements were counted for 10 s on the peak and 5 s on each of two background positions. Sillimanite, albite, almandine, kaersutite, microcline, ilmenite, fluorapatite, scapolite, Ni alloy, cromite, gahnite, bentonite and strontianite mineral standards were employed. Corrections were made using the ZAF method.

Trace element compositions (REE, Ba, Rb, Pb, Th, U, Nb, Ta, Sr, Zr, Hf, Y, Cr, Ni, V and Sc) were determined in situ on >130 μm thick polished sections by laser ablation (LA-ICP-MS) at the University of Bristol using a VG Elemental PlasmaQuad 3 ICP-MS coupled to a VG LaserProbe II (266 nm frequency-quadrupled Nd-YAG laser). Each analysis consisted of 100 s of counting time (including 40 s of background measurement), using a laser beam with a diameter of around 20 μm. NIST 610 glass was used for instrument calibration, and NIST 612 was used as a secondary standard (results are shown in eTable 1). Each analysis was normalised to Ca (clinopyroxene, amphibole, apatite) or Si (feldspars, phlogopite), using concentrations determined by electron microprobe.

Fourteen new whole rock samples were analysed at the CNRS-CRPG Nancy for whole rock major and trace elements, adding to the existing seven dyke analyses (Villaseca et al. 2004; Orejana et al. 2006). The samples were fused using $LiBO_2$ and dissolved with HNO_3. Solutions were analysed by inductively coupled plasma atomic emission spectrometry (ICP-AES) for major elements, whilst trace elements have been determined by ICP mass spectrometry (ICP-MS). Uncertainties in major elements range from 1 to 3%, excepting MnO (5–10%) and P_2O_5 (>10%). Carignan et al. (2001) have evaluated the precision of Nancy ICP-MS analyses at low concentration levels from repeated analysis of the international standards BR, DR-N, UB-N, AN-G and GH. The precision for Rb, Sr, Zr, Y, V, Ga, Hf and most of the REE is in the range 1–5%, whereas they range from 5 to 10% for the rest of trace elements, including Tm. Analyses of BR (an independent standard) are shown in eTable 1.

Pb isotope ratios have been determined on seven lamprophyres and diabases and two hornblenditic xenoliths (previously analysed for Sr–Nd isotope ratios; Villaseca et al. 2004; Orejana et al. 2006) at the Laboratory of Isotope Geology of the Natural History Museum of Stockholm. These samples were dissolved using a 10:1 mixture of HF and HNO_3 according to routine procedures of the laboratory. Pb was separated from the samples using element specific ion-exchange columns. The samples were spiked with a ^{205}Pb tracer solution of known concentration to determine the lead concentrations. Isotope ratios were measured using a Finnigan MAT 261 multicollector TIMS in static mode. Empirical measurements of mass fractionation as a function of temperature were established using the international Pb isotope standards NBS 981 and NBS 982. Data from unknown samples, when corrected in an analogous way, are reproducible and accurate within 0.1% (Table 4) and analyses of BCR-1 gave results ($^{206}Pb/^{204}Pb = 18.79$, $^{207}Pb/^{204}Pb = 15.63$, $^{208}Pb/^{204}Pb = 38.74$) in agreement with literature values ($^{206}Pb/^{204}Pb = 18.81$, $^{207}Pb/^{204}Pb = 15.62$, $^{208}Pb/^{204}Pb = 38.70$).

We are also report Sr–Nd isotopic data for two new lamprophyre samples. These were determined at the

Southampton Oceanography Centre, using a VG Sector 54 multi-collector TIMS with data acquired in multidynamic mode. Isotopic ratios of Sr and Nd were measured on a subsample of whole rock powder. Repeated analysis of NBS 987 gave $^{87}Sr/^{86}Sr = 0.710245 \pm 06$ (2σ) and the $^{143}Nd/^{144}Nd$ ratio of the JM Nd standard was 0.511856 ± 05 (2σ).

Petrography

The SCS alkaline lamprophyres and diabases display a heterogeneous porphyritic texture with abundant mafic phenocrysts (clinopyroxene, kaersutite, olivine pseudomorphs, phlogopite, ulvospinel). Nevertheless, the relative abundance and distribution of these minerals varies significantly from one dyke to another. Following the criteria of Le Maitre et al. (2002) we can classify the SCS lamprophyric dykes (leaving aside diabases) as camptonites, due to the abundance of clinopyroxene, amphibole and phlogopite phenocrysts, absence of felsic phenocrysts and predominance of plagioclase over alkali feldspar within the groundmass. No glass has been found.

Mafic dykes also carry deep-crystallised megacrysts (clinopyroxene, amphibole and plagioclase), which are more abundant in the diabase dykes, and xenoliths of distinctive provenance (wall-rock, lower crustal granulites and pyroxenite xenoliths from the upper mantle-lower crust boundary) (Villaseca et al. 1999; Orejana et al. 2006).

Phenocrysts do not usually exceed 3 mm and vary in their total mode up to 40% in sample 103811. Clinopyroxene and kaersutite are normally zoned, the former sometimes showing multiple rims and oscillatory zoning (Orejana et al. 2007). They are euhedral to subhedral, but may exhibit spongy inner zones infiltrated by groundmass. Fresh olivine has only been observed in one diabase dyke, whereas olivine pseudomorphs, which are mainly transformed to talc group minerals, are common in most lamprophyres and diabases. Plagioclase phenocrysts are only present in diabase dykes, which also occasionally contain mafic phenocrysts. In a analogous fashion to plagioclase, phlogopite phenocrysts are not present in all dykes, but are restricted to some K-rich lamprophyres. Two distinctive spinel phenocrysts are found: black ulvospinel, which transits to Ti-magnetite, and Cr-rich brown spinel microphenocrysts. Other phenocrysts found in variable quantities are ilmenite, apatite and Fe-sulphides.

The groundmass is typically holocrystalline, with a fine-grained inequigranular texture (grain sizes ranging from 10 to 800 μm), although trachytic texture is found in some samples. The main minerals found in the groundmass are clinopyroxene, kaersutite, biotite–phlogopite, Ti–magnetite–ulvospinel, olivine (normally pseudomorphosed), plagioclase and alkali feldspar; with lesser amounts of apatite, analcite, calcite, Fe–sulphides, barite, ilmenite and monazite. These crystals are euhedral to subhedral, with the exception of alkali feldspar, calcite and analcite, which are usually interstitial.

These alkaline rocks show different ocelli and vesicles types: (1) feldspatic, (2) carbonatic and (3) chlorite-rich (with acicular clinopyroxene). Feldspatic ocelli (syenitic) are irregular or semirounded, consisting of kaersutite, biotite and alkali feldspar laths, occasionally showing an inner calcite/analcite globule. Carbonatic ocelli are similar to these calcite globules, with minor amounts of feldspar and chlorite. Chlorite-rich vesicles are outlined by small clinopyroxene crystals that occur as prismatic laths. The inner zone of these ocelli shows chlorite, calcite, albite and minor barite. This kind of ocelli are typical of alkaline lamprophyres and are interpreted as volatile exsolution at shallow emplacement levels (Rock 1991).

Most of the SCS alkaline dykes are remarkably fresh. Alteration of the samples is mainly restricted to pseudomorphed olivine (by talc), although this secondary process is likely to be due to autometasomatism during volatile exsolution. Thus, it is likely that a selective low-P late-magmatic alteration of suspended solids (xenoliths and phenocrysts) occurred during lamprophyric magma devolatilization (Orejana and Villaseca 2008).

Mineral chemistry

Clinopyroxene

The major element composition of representative clinopyroxenes from SCS alkaline basic dykes is summarized in Table 1 (see the whole data on eTable 2). They are Ti-diopsides or Ti-augites, following the criteria of Morimoto et al. (1988). Matrix clinopyroxene is similar in major element composition to phenocrysts, but display lower Mg# values (0.60–0.81) (Fig. 2). Clinopyroxene yields a heterogeneous composition characterized by high TiO_2 and Al_2O_3 concentrations (up to 5.7 and 11.4 wt%, respectively). Na_2O content ranges from 0.33 to 1.10 wt% and Cr_2O_3 may reach up to 0.9 wt%. Normal zoning is relatively common in the phenocrysts, and it gives trends of increasing Fe, Al, Ti and Ca concentrations and decreasing Mg#, Si and Cr from core to rim (Orejana et al. 2007). Clinopyroxene phenocrysts exhibit high concentrations of most trace elements (eTable 3): REE (48–120 ppm), LILE (Rb = 0.6–5.9 ppm; Ba = 1.5–3.6 ppm) and HFSE (Th = 0.1–0.4 ppm; Ta = 0.1–0.7 ppm; Nb = 0.5–1.6 ppm; Zr = 43–153 ppm). They display convex upward

Table 1 Representative major element composition of clinopyroxene and amphibole from SCS alkaline lamprophyres and diabases

Mineral	Clinopyroxene									Amphibole										
Type	Phenocrysts						Matrix			Phenocrysts					Matrix				Ocelli	
Sample #	10212931	103474	10381160	10381162	10347391	10347392	10189215	102147A	10440332	803189	103333B21	10347398	10347399	10347104	10189215	10347312	10440335	U3734	104534A21	10455116
	core	core	core	rim	core	rim		79		core	core	core	rim	core	5	5				
SiO_2	45.97	45.48	48.09	43.90	46.91	45.75	44.62	50.27	44.41	38.38	39.27	38.63	39.01	38.37	39.38	38.50	37.12	38.24	38.32	40.88
TiO_2	3.53	2.51	1.43	3.98	2.50	2.62	4.40	1.50	3.07	6.50	5.29	6.09	6.32	6.13	5.35	6.74	7.89	3.56	6.03	3.33
Al_2O_3	7.28	8.32	5.55	7.56	8.42	8.87	7.19	2.45	9.67	14.19	13.22	13.78	13.87	13.84	11.33	12.87	13.77	14.06	13.06	9.20
FeO[a]	7.90	5.49	4.76	6.29	4.62	6.61	9.10	10.32	7.10	11.18	11.03	11.62	9.11	10.07	16.56	9.48	9.33	18.97	12.68	23.37
Cr_2O_3	0.00	0.07	0.20	0.18	0.05	0.04	0.00	0.02	0.17	0.00	0.00	0.00	0.01	0.05	0.00	0.00	0.00	0.00	0.00	0.00
MnO	0.07	0.06	0.09	0.13	0.08	0.01	0.14	0.20	0.13	0.26	0.08	0.05	0.01	0.07	0.21	0.11	0.16	0.35	0.28	0.42
MgO	11.17	13.29	15.40	12.66	13.66	12.80	11.10	11.68	12.45	12.50	11.79	11.53	13.16	12.31	9.04	12.99	12.43	7.46	11.04	5.06
CaO	22.82	22.83	22.64	24.02	22.28	22.13	22.20	22.09	23.16	11.61	11.74	11.83	12.25	11.92	11.37	12.11	13.45	11.26	11.93	11.13
Na_2O	0.57	0.68	0.61	0.38	0.67	0.77	0.58	0.55	0.75	2.07	2.06	1.82	1.83	2.03	2.85	2.09	1.95	2.43	2.49	2.71
K_2O	0.00	0.00	0.00	0.00	0.01	0.00	0.02	0.01	0.00	2.07	1.93	2.26	2.24	2.10	0.87	1.66	1.52	1.68	1.65	1.65
Total	99.31	98.72	98.77	99.10	99.20	99.60	99.35	99.09	100.91	98.76	96.41	97.61	97.81	96.89	96.96	96.55	97.62	98.01	97.48	97.75
Mg#	0.72	0.81	0.85	0.80	0.84	0.78	0.69	0.67	0.76	0.67	0.66	0.64	0.72	0.69	0.49	0.71	0.70	0.41	0.61	0.28
Cations calculated on the basis of 6 O for clinopyroxene and 24 (O, OH, F) for amphibole																				
Si	1.734	1.693	1.776	1.646	1.734	1.694	1.690	1.910	1.628	5.658	5.958	5.813	5.806	5.790	6.077	5.812	5.628	5.865	5.824	6.508
Ti	0.100	0.070	0.040	0.112	0.070	0.073	0.125	0.043	0.085	0.721	0.604	0.689	0.707	0.696	0.621	0.765	0.900	0.411	0.689	0.399
Al	0.323	0.365	0.241	0.334	0.366	0.387	0.321	0.110	0.417	2.463	2.362	2.442	2.431	2.459	2.058	2.288	2.459	2.540	2.338	1.724
Fe	0.249	0.171	0.147	0.197	0.143	0.204	0.288	0.328	0.218	1.379	1.400	1.462	1.134	1.271	2.137	1.197	1.183	2.433	1.612	3.111
Cr	0.000	0.002	0.006	0.005	0.001	0.001	0.000	0.001	0.005	0.000	0.000	0.000	0.001	0.006	0.000	0.000	0.000	0.000	0.000	0.000
Mn	0.002	0.002	0.003	0.004	0.003	0.000	0.004	0.006	0.004	0.032	0.010	0.006	0.001	0.009	0.027	0.014	0.021	0.045	0.036	0.057
Mg	0.628	0.738	0.848	0.708	0.753	0.707	0.627	0.662	0.680	2.747	2.667	2.587	2.920	2.769	2.080	2.923	2.810	1.706	2.501	1.201
Ca	0.922	0.911	0.896	0.965	0.882	0.878	0.901	0.899	0.910	1.834	1.908	1.907	1.953	1.927	1.880	1.959	2.185	1.850	1.943	1.898
Na	0.042	0.049	0.044	0.028	0.048	0.055	0.043	0.040	0.053	0.591	0.606	0.531	0.528	0.594	0.852	0.612	0.573	0.723	0.733	0.837
K	0.000	0.000	0.000	0.000	0.000	0.000	0.001	0.001	0.000	0.389	0.374	0.434	0.425	0.404	0.171	0.320	0.294	0.329	0.320	0.335
Cations sum.	4.000	4.001	4.002	3.999	4.000	3.999	4.000	4.000	4.000	15.814	15.889	15.871	15.906	15.925	15.903	15.890	16.053	15.902	15.996	16.070

[a] Total Fe expressed as FeO

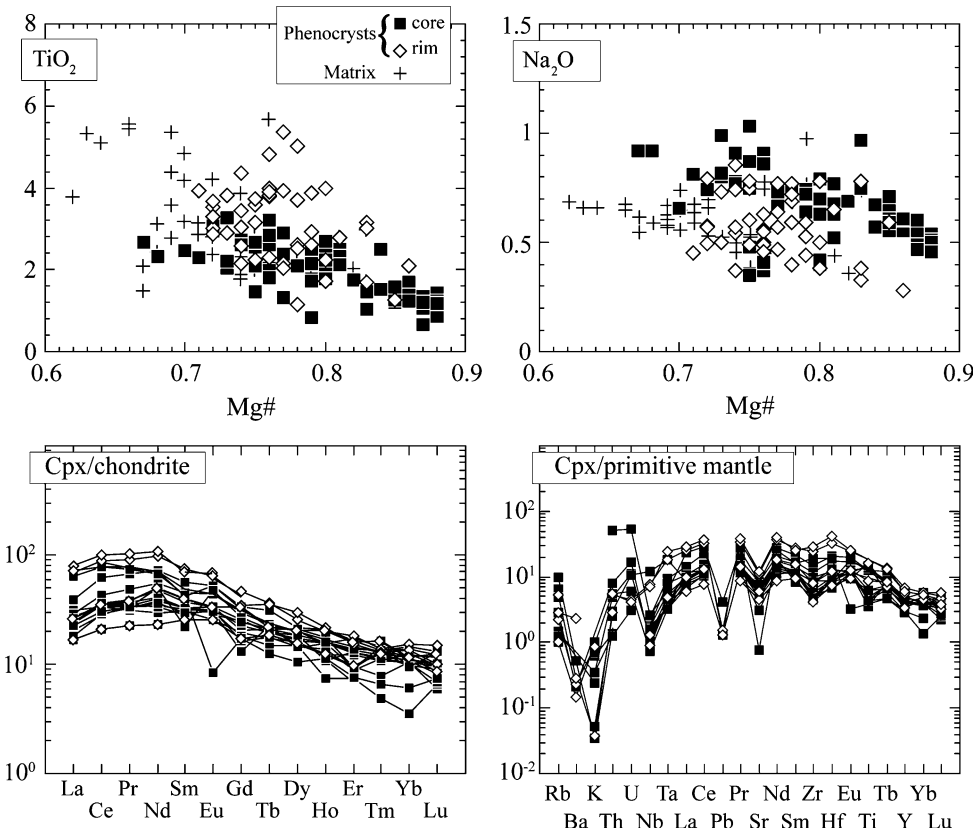

Fig. 2 Major and trace element composition of clinopyroxene from the SCS alkaline basic dykes. The normalising values of chondrite and primitive mantle are after Sun and McDonough (1989) and McDonough and Sun (1995), respectively

chondrite-normalised REE patterns (Fig. 2), similarly to clinopyroxenes crystallized at depth from basaltic melts (Irving and Frey 1984). Negative Ba, K, Nb, Pb and Sr anomalies may be found in their primitive mantle-normalised trace element patterns.

Amphibole

The major element composition of representative amphiboles from SCS alkaline basic dykes is summarized in Table 1 (see the whole data on eTable 4). They are classified as kaersutites according to Leake et al. (1997). These amphiboles are Al–Ti-rich, with Al_2O_3 up to 14.8 wt% and TiO_2 up to 7.7 wt% (Fig. 3). Phenocrysts show a homogeneous composition, with Mg# in the range 0.61–0.72. Matrix amphiboles overlap phenocrysts composition, but generally have more evolved compositions resembling the major element composition of amphibole from feldspatic ocelli (Fig. 3). Amphibole trace element compositions (eTable 3) mimic those of coexisting clinopyroxene phenocrysts, with characteristic convex upward chondrite-normalised REE patterns (Fig. 3). Nevertheless they show a slight enrichment in most trace elements with respect to clinopyroxene. They have high Ba (537–826 ppm), Nb (40–126 ppm), Ta (2.3–5.6 ppm) and Sr (>1,150 ppm) concentrations, this is reflected in positive anomalies for these elements in primitive mantle-normalised patterns.

Olivine

Fresh olivine is only present in a scarce group of diabases (both as phenocrysts and within the groundmass). Nevertheless, the abundance of pseudomorphs in most SCS alkaline dykes highlights its potential importance during crystal fractionation. Forsterite content varies from Fo_{77} to Fo_{90} in phenocrysts (including slightly Fe-rich rims) (eTable 5). These values match the Mg/Fe ratios of clinopyroxene phenocrysts (0.67–0.88), indicating equilibrium crystallization. Olivine Mg# correlates positively with NiO content (0.05–0.28 wt%) (eFig. 1). Matrix olivine compositions overlaps those of phenocrysts, but they extend towards lower Mg (Fo_{75}–Fo_{83}) and NiO (0.05–0.13 wt%) concentrations.

Micas

They constitute a heterogeneous group ranging from Ti-biotite to Ti-phlogopite, whose main characteristic is high TiO_2 (up to 10.5 wt%) and Al_2O_3 (up to 17.8 wt%)

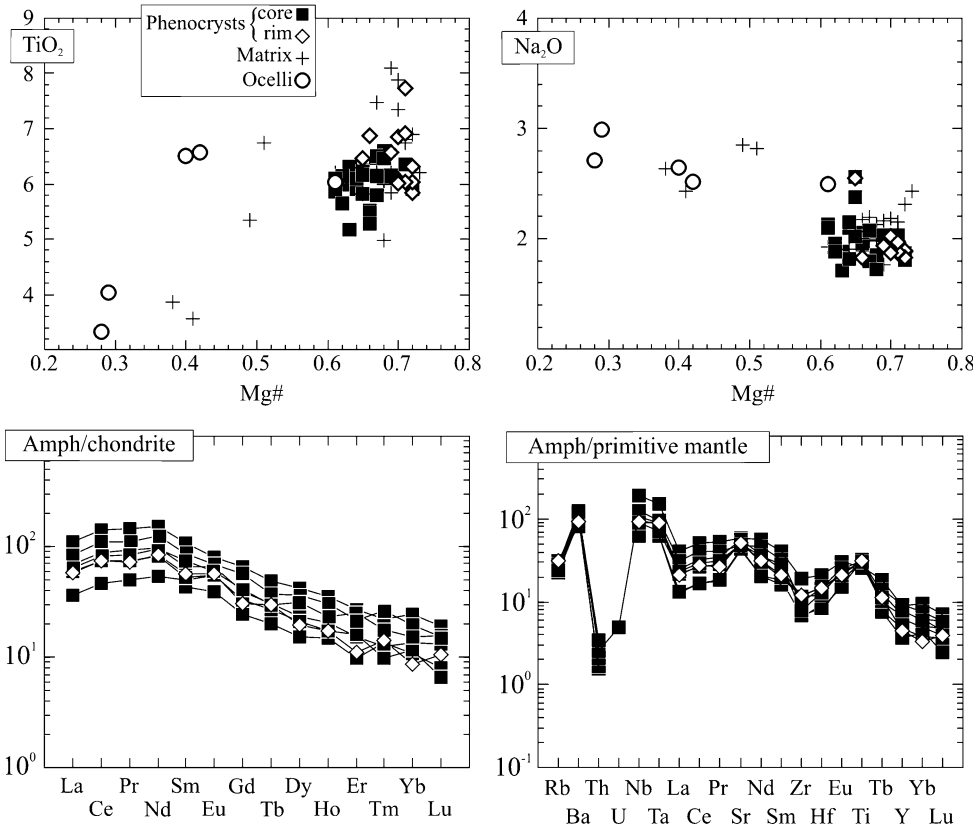

Fig. 3 Major and trace element composition of amphibole from the SCS alkaline basic dykes. The normalising values of chondrite and primitive mantle are after Sun and McDonough (1989) and McDonough and Sun (1995), respectively

(eFig. 1; Table 2 and eTable 6). Similar to amphibole, mica phenocrysts (which are mainly phlogopites) display high Mg# values (0.65–0.78) and major element concentrations similar to those of groundmass micas, with the exception of Mg#, which may be as low as 0.28 in the matrix, resembling composition of biotites from feldspatic ocelli (eFig. 1). They may also have high F concentrations (up to 3.4%). Phlogopite phenocrysts exhibit high trace element concentrations (eTable 3), notably Ba (3,000–6,000 ppm), Rb (280–360 ppm), Nb (15–50 ppm) and Ta (0.9–2.2 ppm). These compositions are very similar to those of phlogopite phenocrysts from other alkaline lamprophyres (Foley et al. 1996) (eFig. 1).

Feldspars

The major element composition of representative feldspars (plagioclases and alkali feldspar) in SCS alkaline dykes is summarized in eTable 7. Phenocrysts are exclusively plagioclases (from andesine to labradorite, An_{32}–An_{70} (eFig. 2)) and are restricted to diabase dykes. The compositional field of groundmass feldspars is wider, with plagioclases overlapping the phenocrysts range, but plotting towards more albite and orthoclase-rich compositions, and alkali feldspar falling within the sanidine compositional field (Or_{54}–Or_{100}). Plagioclase phenocrysts are usually zoned with core compositions of $An_{61–70}$ and rims of $An_{49–62}$ (eFig. 2).

Other minerals

Spinel compositions are shown in eTable 5. Phenocrysts are Ti–magnetite–ulvospinel and Cr-spinel. The first group is more abundant and displays a relatively heterogeneous composition with FeO + Fe_2O_3 = 52–76 wt% and TiO_2 in the range 12–36 wt%, whilst Al_2O_3 and MgO do not exceed 9 and 3 wt%, respectively (eFig. 3). Cr-spinels are euhedral and always overgrown by ulvospinel rims. Their Cr_2O_3 and Al_2O_3 concentrations range from 10 to 38 wt% and from 28 to 52 wt%, respectively. A negative correlation exists between Al and Cr (Mg) contents. Groundmass spinels are restricted to Ti–magnetite–ulvospinel series and overlap the compositional field of ulvospinel phenocrysts, although they tend towards slightly Fe-enriched compositions (eFig. 3).

Apatite may appear as phenocrysts or within the matrix. This phase is always F-rich (1.4–2.7 wt%) (eTable 5) and is classified as fluorapatite. Cl does not exceed 0.5 wt% and SrO ranges from 0.01 to 0.35 wt%. Ilmenite is restricted to the San Bartolomé de Pinares dyke and it is characterized by high MgO (0.02–10 wt%) and MnO (0.5–10 wt%) (eTable 5). Mg–Mn-rich ilmenites have been proposed by

Table 2 Representative major element composition of micas and olivine from SCS alkaline lamprophyres and diabases

Mineral	Mica								Olivine					
Type	Phenocrysts				Matrix		Ocelli		Phenocrysts				Matrix	
Sample	80318-53	103474-25	103684-107	103473-123	101892-138	103811-67	102129-37	104551-11	101892A-60 core	101892A-62 rim	101892A-68 core	104867-57 core	101892-119	101892-129
SiO_2	35.77	34.82	35.51	36.91	34.10	34.73	34.77	35.96	40.34	40.31	38.80	38.78	37.62	38.47
TiO_2	8.85	8.66	7.65	6.68	7.64	8.48	8.19	4.54	0.00	0.03	0.05	0.02	0.03	0.01
Al_2O_3	16.51	16.05	14.48	15.12	13.48	15.65	14.00	12.65	0.08	0.15	0.05	0.07	0.01	0.04
Cr_2O_3	0.10	0.03	0.00	0.13	0.00	0.03	0.00	0.02	NA	NA	NA	NA	NA	NA
FeO[a]	8.98	9.66	11.05	12.03	24.00	10.51	18.14	23.55	9.99	18.12	20.05	12.96	25.36	17.94
NiO	NA	NA	NA	NA	NA	NA	NA	NA	0.28	0.09	0.06	0.28	0.00	0.11
MnO	0.01	0.04	0.12	0.01	0.22	0.04	0.09	0.17	0.28	0.39	0.42	0.20	0.26	0.22
MgO	16.93	15.14	15.45	14.71	5.88	14.87	9.80	9.09	49.20	39.99	41.25	46.54	36.44	41.61
CaO	0.00	0.25	0.04	0.05	0.02	0.10	0.03	0.07	0.30	0.24	0.25	0.28	0.16	0.14
NA $_2$O	0.42	0.65	0.55	0.69	0.52	0.53	0.78	0.45	0.00	0.04	0.03	0.00	0.03	0.02
K_2O	9.57	8.21	8.75	9.47	8.46	8.39	8.29	8.81	0.02	0.00	0.00	0.00	0.00	0.01
BaO	0.00	0.69	1.34	0.19	0.00	1.29	0.00	0.03	NA	NA	NA	NA	NA	NA
F	NA	0.00	0.49	1.28	NA	0.36	NA	0.17	NA	NA	NA	NA	NA	NA
Total	97.14	94.20	95.43	97.27	94.32	94.98	94.09	95.51	100.49	99.36	100.96	99.13	99.91	98.56
Mg#	0.77	0.74	0.71	0.68	0.30	0.72	0.49	0.41	0.90	0.80	0.79	0.87	0.72	0.81
Cations calculated on the basis of 24 (O, OH, F, Cl) for mica and 4 O for olivine														
Si	5.360	5.400	5.550	5.670	5.660	5.420	5.610	5.880	0.988	1.031	0.990	0.978	0.995	0.996
Ti	1.000	1.010	0.900	0.770	0.950	1.000	0.990	0.560	0.000	0.001	0.001	0.000	0.001	0.000
Al	2.915	2.934	2.665	2.738	2.637	2.876	2.660	2.436	0.002	0.005	0.002	0.002	0.000	0.001
Cr	0.010	0.000	0.000	0.020	0.000	0.000	0.000	0.000	0.000	0.000	0.000	0.000	0.000	0.000
Fe	1.130	1.250	1.440	1.550	3.330	1.370	2.450	3.220	0.205	0.388	0.428	0.273	0.561	0.388
Ni	0.000	0.000	0.000	0.000	0.000	0.000	0.000	0.000	0.006	0.002	0.001	0.006	0.000	0.002
Mn	0.000	0.010	0.020	0.000	0.030	0.010	0.010	0.020	0.006	0.008	0.009	0.004	0.006	0.005
Mg	3.780	3.500	3.600	3.370	1.460	3.460	2.360	2.220	1.796	1.525	1.569	1.750	1.437	1.606
Ca	0.000	0.040	0.010	0.010	0.000	0.020	0.010	0.010	0.008	0.007	0.007	0.008	0.005	0.004
Na	0.120	0.200	0.170	0.210	0.170	0.160	0.240	0.140	0.000	0.002	0.001	0.000	0.002	0.001
K	1.830	1.630	1.740	1.860	1.790	1.670	1.710	1.840	0.001	0.000	0.000	0.000	0.000	0.000
Ba	0.000	0.040	0.080	0.010	0.000	0.080	0.000	0.000	0.000	0.000	0.000	0.000	0.000	0.000
Cations sum.	16.145	16.014	16.175	16.208	16.027	16.066	16.040	16.326	3.012	2.969	3.008	3.021	3.007	3.003

[a] Total Fe expressed as FeO. *NA* not analised

Rock (1991) as a diagnostic feature of alkaline lamprophyres.

Whole-rock geochemistry

Major and trace elements

The major and trace element composition of the SCS alkaline dykes is shown in Table 3. Although all samples have high LOI numbers (mainly 2.9–5.7 wt%), due to the abundance of hydrous minerals (amphibole and phlogopite), those displaying the highest values correspond with ocelli-rich varieties.

Due to their silica and alkalis contents (ranging from 41.2 to 47.4 wt% and from 3.0 to 7.4 wt%, respectively; Table 3) the SCS lamprophyres and diabases plot within the alkaline area in the TAS diagram (taken from Le Bas et al. 1986), mainly within the basanite compositional field. The K_2O/Na_2O ratio of the lamprophyres (a parameter used to differentiate potassic from sodic rocks) is higher than unity (Fig. 4) (Le Bas et al. 1986; Le Maitre et al. 2002), whereas the diabases are sodic. Nevertheless, two lamprophyre samples which yield $K_2O/Na_2O > 2$ could be included within an ultrapotassic group, following the criteria of Foley et al. (1987) and Le Maitre et al. (2002) (Fig. 4). Apart from being high in K, they are characterized by high TiO_2 (1.4–4.1 wt%) and P_2O_5 (0.28–1.0 wt%) concentrations and moderate to low Mg# (0.43–0.7) (Table 3).

These alkaline dykes are markedly heterogeneous in their major and trace element composition (e.g. MgO = 4.5–12.2 wt%; Al_2O_3 = 10.3–16.8 wt%; CaO = 5–13 wt%; Rb = 46–145 ppm; Zr = 112–367 ppm; Y = 22–66 ppm) (Table 3). The diabases can be differentiated from lamprophyres due to their lower K–Ti–Ta–Zr–Hf–V and higher Mn–Cs contents (Fig. 5). When considered separately, samples from a single dyke usually show compositional variations characterized by an increase in Si, Al, Na, K and most incompatible trace elements, and a decrease of Ti, Ca, Cr, Ni and V towards lower Mg# (Fig. 5).

The dykes are also characteristically enriched in incompatible trace elements. The REE are fractionated showing steep chondrite-normalised patterns with highly enriched LREE and depleted HREE (Fig. 6). The chondrite-normalised values are between 100 and 400 with respect to the La content, whereas Yb and Lu values are predominantly <20. This is reflected in their high $(La/Yb)_N$ values from 9.6 to 23.3. LILE and HFSE also display high concentrations, giving rise to positive Rb–Ba and Nb–Ta anomalies in primitive mantle-normalised patterns (Fig. 6). It is also worth noting the K peak and the Th–U and Pb troughs. These compositions resemble those of OIB, but show higher Rb, Ba, Th, U, K, Nb and Ta contents.

Sr–Nd–Pb isotope ratios

All isotopic data for SCS alkaline lamprophyres and diabases are corrected to 265 Ma (Table 4), taking into consideration the most recent geochronological results. Figure 7 shows both the new Sr–Nd analyses presented in this work and those recently obtained by our research group (Villaseca et al. 2004; Orejana et al. 2006). The data overlap the wide compositional field of OIB, falling within the mantle array. The most radiogenic compositions partially coincide with previous data from Bea et al. (1999) and Perini et al. (2004), confirming the marked heterogeneous composition of these Permian intrusive rocks, as previously suggested by Villaseca et al. (2004) and Orejana et al. (2006). This heterogeneity allows us to differentiate two groups: (1) one isotopically depleted, plotting close to MORB compositions and with $(^{87}Sr/^{86}Sr)_0$ in the range 0.7023–0.7038 and εNd_0 in the range +4.0 to +7.1, and (2) an isotopically enriched group, resembling bulk silicate earth (BSE) isotopic values, with $(^{87}Sr/^{86}Sr)_0$ ranging from 0.7044 to 0.7052 and εNd_0 from −0.9 to +1.4 (Fig. 7). All diabases and an ultrapotassic lamprophyre from the Sierra de la Paramera dyke plot within the depleted group. The isotopically enriched group corresponds to camptonitic dykes. There is a close resemblance between the Sr–Nd isotopic composition of the SCS alkaline basic dykes and that of the most depleted alkaline rocks from western Europe Permo-Carboniferous magmatism (Fig. 7), this is discussed below.

The Pb isotope analyses display more restricted compositional variation with $(^{206}Pb/^{204}Pb)_0$ = 18.16–18.51, $(^{207}Pb/^{204}Pb)_0$ = 15.54–15.64 and $(^{208}Pb/^{204}Pb)_0$ = 37.93–38.44 (Table 4). The only previous Pb isotope data available on the SCS alkaline dykes is that of Perini et al. (2004), these rocks belong to the Sr–Nd isotopically enriched group of lamprophyres (Fig. 8). Overall, the Pb isotope compositions are close to PREMA (Prevalent Mantle) and BSE (mainly when considering $^{206}Pb/^{204}Pb$), although they display some tendency towards being slightly ^{207}Pb and ^{208}Pb-enriched. Nevertheless, the Pb radiogenic ratios indicate derivation from a relatively depleted source. When considered in detail, the same division made on the basis of Sr–Nd isotope ratios can also be made on the basis of Pb isotope ratios; the Sr–Nd isotopically enriched lamprophyres clearly display the most radiogenic Pb values within the narrow compositional range of SCS alkaline dykes (Fig. 8). Absence of highly radiogenic Pb data implies that the PREMA component (and not HIMU) is dominant in the isotopically depleted SCS alkaline group (Orejana et al. 2005). A similar

Table 3 Major and trace element composition of SCS alkaline lamprophyres and diabases

	Lamprophyres									
Dyke	Maragato	Puerto del Pico		Villatoro	Paramera		San Bartolomé de Pinares	Tornadizos-Ávila		
Sample	103811	103818	103681	103333A	76547	77753[a]	104541[b]	80318	103474	103473[a]
GC[c]	UK 286775	UK 258893	UK 289655	UK 151890	UK 433819	UK 433819	UK 703879	UK 660973	UK 660973	UK 660973
SiO_2	43.84	44.91	44.82	47.44	42.62	41.20	43.96	43.59	45.37	45.66
TiO_2	3.09	3.71	3.72	3.47	2.47	2.75	2.85	4.09	3.68	3.61
Al_2O_3	10.34	13.98	15.72	15.23	14.40	13.28	14.67	16.17	16.49	16.68
Fe_2O_3[d]	10.14	11.44	11.18	11.32	3.18	12.33	10.25	12.23	12.42	12.39
FeO	NA	NA	NA	NA	7.32	NA	NA	NA	NA	NA
MnO	0.13	0.17	0.16	0.15	0.17	0.16	0.13	0.12	0.13	0.12
MgO	12.22	7.63	6.04	6.07	10.78	11.05	7.83	5.83	5.37	4.91
CaO	12.91	7.91	6.82	5.52	9.81	10.24	8.32	5.95	5.89	5.07
Na_2O	1.31	2.30	2.83	2.89	2.09	1.18	2.31	1.60	3.17	2.97
K_2O	1.69	3.59	3.90	3.77	2.58	3.52	3.79	4.26	3.86	4.39
P_2O_5	0.28	0.43	0.38	0.43	0.51	0.58	0.72	0.75	0.74	0.78
LOI	3.99	3.53	4.50	3.69	3.70	3.31	5.29	4.22	2.92	3.58
Total	99.94	99.60	100.07	99.98	99.63	99.60	100.12	98.81	100.04	100.16
Mg#	0.70	0.57	0.52	0.51	0.65	0.64	0.60	0.49	0.46	0.44
Ba	1353	1429	1083	1078	968	854	1425	1021	1203	2475
Rb	48.9	107	145	113	46	74	115	132	105	137
Cs	4.31	1.51	3.75	2.11	NA	NA	6.49	NA	3.68	5.5
Sr	514	631	705	591	536	585	1266	781	923	803
Pb	2.96	4.67	5.19	5.1	NA	3.28	6.09	NA	6.24	6.56
Th	2.65	5.17	4.98	5.96	NA	5	6.94	6	6.25	6.21
U	0.64	1.03	1.12	1.55	NA	1.32	1.82	NA	1.63	1.75
Zr	177	241	274	283	112	167	356	329	355	367
Nb	45.7	74.7	79.3	86.6	NA NA	69	107	110	107	110
Y	42.5	24.2	25.6	26.8	31	25	23.5	43	54.2	66.2
Sc	NA	NA	NA	NA	NA	34	NA	31	NA	NA
Co	47.2	36.2	31.5	30	NA	48	34.4	32	36.7	34.1
V	288	321	296	354	NA	280	256	420	384	377
Ni	103	55.8	27	18.6	165	176	103	40	25	22.5
Cr	767	183	66.4	52.4	NA	415	272	60	40.6	35.4
Cu	25.3	44.9	21.6	39.4	NA	80	39.2	44	30.5	28.7
Zn	75.8	102	112	116	NA	83	95.9	90	107	110
Ga	15.9	20.4	20.9	21.6	10	22	20.1	27	22.2	22.5
Ta	3.81	6.14	6.57	6.62	NA	NA	8.52	NA	8.69	8.87
Hf	4.76	6.05	6.3	6.76	NA	NA	7.47	NA	7.99	7.61
La	29.1	40.9	43.6	53.2	50	39.7	61.3	96	69.3	82.3
Ce	54.4	84.3	85.5	108	56	69.7	120	118.5	128	137
Pr	7.8	10.1	10.4	12.9	NA	NA	13.6	NA	17.8	21.3
Nd	33.2	39.6	40.8	49.3	NA	35.2	50.9	74.2	72.3	84.4
Sm	7.07	7.37	7.62	8.49	NA	7.12	8.69	14.91	13.4	16.9
Eu	2.07	2.11	2.43	2.6	NA	2.27	2.82	3.56	3.93	4.64
Gd	7.31	6.02	6.31	7.04	NA	6.56	6.85	11.37	11.9	14.6
Tb	1.01	0.86	0.92	0.98	NA	NA	0.88	NA	1.73	2.11
Dy	5.56	4.72	4.84	5.39	NA	4.9	4.82	8.57	9.31	11.9

Table 3 continued

	Lamprophyres										
Dyke	Maragato	Puerto del Pico		Villatoro	Paramera		San Bartolomé de Pinares	Tornadizos-Ávila			
Sample	103811	103818	103681	103333A	76547	77753[a]	104541[b]	80318	103474	103473[a]	
GC[c]	UK 286775	UK 258893	UK 289655	UK 151890	UK 433819	UK 433819	UK 703879	UK 660973	UK 660973	UK 660973	
Ho	1.1	0.85	0.88	1.03	NA	NA	0.83	NA	1.9	2.44	
Er	2.91	2.28	2.33	2.51	NA	2.39	2.25	3.89	4.56	5.85	
Tm	0.37	0.32	0.34	0.34	NA	NA	0.31	NA	0.61	0.79	
Yb	2.17	2.08	2.19	2.4	NA	1.84	2.03	2.96	3.86	5.25	
Lu	0.32	0.32	0.34	0.36	NA	0.22	0.29	0.35	0.57	0.77	

	Lamprophyres						Diabases				
Dyke	Hoyo de Pinares						Bernuy Salinero			Peguerinos	
Sample	103673	76543	78846	103674[a]	76542	78850	U-37	81843	81839[b]	81938[a]	101892[b]
GC[c]	UK 813816	UK 816812	UK 862729	UK 813816	UK 816812	UK 682881	UK 645784	UL 645035	UL 656048	UK 950982	UK 950982
SiO_2	43.57	43.43	42.38	43.62	43.40	44.29	42.72	46.28	43.94	46.96	42.45
TiO_2	2.46	3.41	3.56	3.36	3.27	3.16	1.98	1.43	2.30	1.86	2.39
Al_2O_3	14.18	14.26	15.70	15.21	15.29	15.58	15.21	16.16	15.98	16.81	16.04
Fe_2O_3[d]	11.62	11.92	4.02	11.82	11.66	11.08	12.33	10.56	12.34	11.83	11.99
FeO	NA	NA	6.91	NA	NA	NA	NA	NA	NA	NA	NA
MnO	0.15	0.16	0.14	0.15	0.15	0.17	0.19	0.19	0.19	0.15	0.19
MgO	8.44	7.94	7.52	7.00	6.69	5.83	6.88	5.74	5.74	4.50	5.95
CaO	10.13	9.80	8.47	8.57	8.45	7.85	9.01	7.62	8.49	5.95	8.62
Na_2O	2.40	2.50	3.17	2.66	2.83	2.51	3.54	3.01	3.14	3.13	3.14
K_2O	2.48	2.92	3.67	3.10	3.16	4.71	1.67	2.79	2.98	2.58	1.75
P_2O_5	0.43	0.56	1.00	0.53	0.54	0.42	0.77	0.57	1.00	0.61	0.43
LOI	3.51	3.52	3.19	4.00	4.57	4.43	5.37	5.67	3.31	5.28	7.05
Total	99.37	100.42	99.73	100.02	100.01	100.03	99.67	100.02	99.41	99.66	100.00
Mg#	0.59	0.57	0.56	0.54	0.53	0.51	0.53	0.52	0.48	0.43	0.50
Ba	809	769	1157	963	818	1194	505	932	947	576	616
Rb	62.9	80	74	91.4	90.7	116	75	109	129	54	56.5
Cs	6.51	NA	NA	8.44	7.84	3.86	NA	45.1	75.7	NA	56.1
Sr	716	776	987	880	814	989	619	860	942	633	1387
Pb	4.06	NA	NA	5.47	6.07	49	NA	5.18	3.65	NA	4.56
Th	4.04	6	bdl	5.26	4.8	5.35	8	7.56	6.42	5	4.01
U	0.97	NA	NA	1.19	1.25	1.4	NA	2.49	1.87	NA	1.02
Zr	210	215	182	263	246	290	185	214	216	214	174
Nb	61.6	69	NA	81.5	77.7	79.1	85	74.2	96.8	59	49.1
Y	23.7	24	25	24.6	23.3	22.2	32	30.8	28.5	30	27
Sc	NA	33.9	NA	NA	NA	NA	23.7	NA	17	16.29	NA
Co	41.2	37	NA	43	40.1	34.5	29	29.5	32	17	36
V	323	342	NA	329	322	240	190	130	152	111	159
Ni	82.3	90	58	77.2	72.2	55.6	86	94.9	53	49	53.5
Cr	258	285	NA	227	213	167	245	283	142	214	118
Cu	42.6	51	NA	40.3	39.8	37.1	59	39	36	45	37.9
Zn	91.9	78	NA	106	98.4	156	72	88.2	86	69	75.1
Ga	17.7	25	11	20.4	19.7	21	21	17.4	18	20	16.5
Ta	4.99	NA	NA	6.34	6.45	7.01	NA	5.44	6.01	NA	3.52

Table 3 continued

	Lamprophyres						Diabases				
Dyke	Hoyo de Pinares						Bernuy Salinero			Peguerinos	
Sample	103673	76543	78846	103674[a]	76542	78850	U-37	81843	81839[b]	81938[a]	101892[b]
GC[c]	UK 813816	UK 816812	UK 862729	UK 813816	UK 816812	UK 682881	UK 645784	UL 645035	UL 656048	UK 950982	UK 950982
Hf	5.16	NA	NA	5.85	5.74	6.5	NA	4.87	5.4	NA	3.83
La	34.4	38.6	70	44	42.9	43.5	53.8	54.1	56.1	40.4	55.3
Ce	71.3	72.2	92	92.1	84.9	87.7	94.6	93.7	104	71.6	104
Pr	8.4	NA	NA	10.4	10.2	10.3	NA	10.1	11.5	NA	11.3
Nd	36.5	37.7	NA	42.9	39.1	40.2	39.8	37.6	46.5	31.7	42.2
Sm	7	7.83	NA	7.45	7.04	7.75	8.02	6.71	8.91	6.91	7.65
Eu	2.29	2.32	NA	2.43	2.32	2.52	2.52	2.19	2.94	2.19	2.44
Gd	6.61	6.38	NA	6.54	6.14	6.58	7.05	6.18	7.52	6.06	6.65
Tb	0.86	NA	NA	0.94	0.9	0.9	NA	0.93	1.21	NA	0.93
Dy	4.56	4.86	NA	4.76	4.68	5	5.86	5.56	6.06	5.27	5.16
Ho	0.84	NA	NA	0.89	0.86	0.8	NA	1.11	1.06	NA	0.97
Er	2.22	2.53	NA	2.33	2.1	2.07	3.49	3.13	3.3	3.37	2.56
Tm	0.31	NA	NA	0.32	0.32	0.3	NA	0.48	0.45	NA	0.38
Yb	2.03	1.84	NA	2.11	1.92	1.74	2.77	3.06	2.75	2.54	2.42
Lu	0.29	0.22	NA	0.33	0.3	0.28	0.36	0.45	0.41	0.33	0.38

[a] Analyses taken from Villaseca et al. (2004)

[b] Analyses taken from Orejana et al. (2006)

[c] *GC* geographic co-ordenates; all samples are within the 30T zone of the Universal Transverse Mercator co-ordinate system

[d] Total Fe expressed as Fe_2O_3, with the only exception of samples 76547 and 78846. *NA*: not analysed. bdl: below detection limit

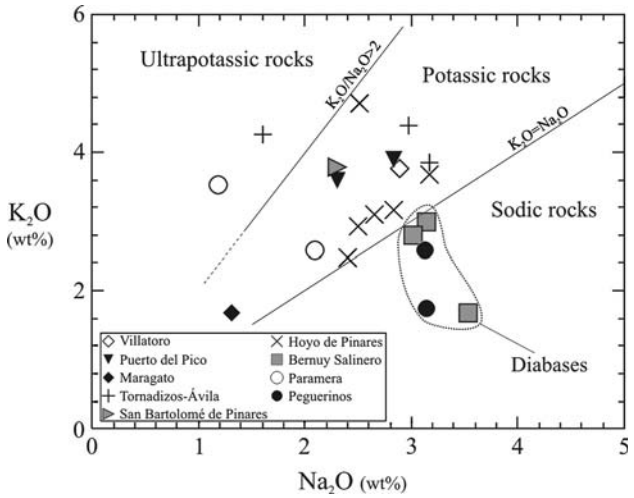

Fig. 4 K_2O versus Na_2O (wt%) contents of the SCS alkaline basic dykes. The *line* for $K_2O/Na_2O > 2$, which separates potassic from ultrapotassic rocks has been constructed with the criteria of Foley et al. (1987)

composition is observed in the Permian alkaline basic dykes from the western Alps (Fig. 8).

The Sr–Nd–Pb isotopic composition of the SCS alkaline magmatism represents the irruption of a new mantle-derived component in the Central-Iberian Zone. The PREMA-like alkaline dykes contrast with the previous calc-alkaline Hercynian basic magmatic suites (Gb1, Gb2 and Gb3; Villaseca et al. 2004) that are clearly lithosphere-derived ($^{87}Sr/^{86}Sr_0$ ranging from 0.7045 to 0.7087 and εNd_0 from −3.9 to +0.6; Fig. 7). This new component is not recorded previously in the whole Hercynian Iberian Massif, suggesting a significant geodynamic change during post-Hercynian times, this is discussed in more detail below.

Petrogenesis

Magma differentiation

One of the main features of the SCS Permian alkaline magmatism is its chemical and petrological heterogeneity, giving rise to the lamprophyre-diabase division and variable phenocryst modal composition. These characteristics are also manifested in the absence of a unique variation trend for the group of dykes as a whole for many major and trace elements (e.g. Ti, K, V, Rb, Zr), although there are both negative and positive correlations between these elements and Mg# when considering the samples of each dyke separately (Fig. 5). This heterogeneity could be explained by the intrusion of several magma batches derived from slightly different mantle sources, or it might be caused by variable amounts of melting. We regard the Sr–Nd isotopic

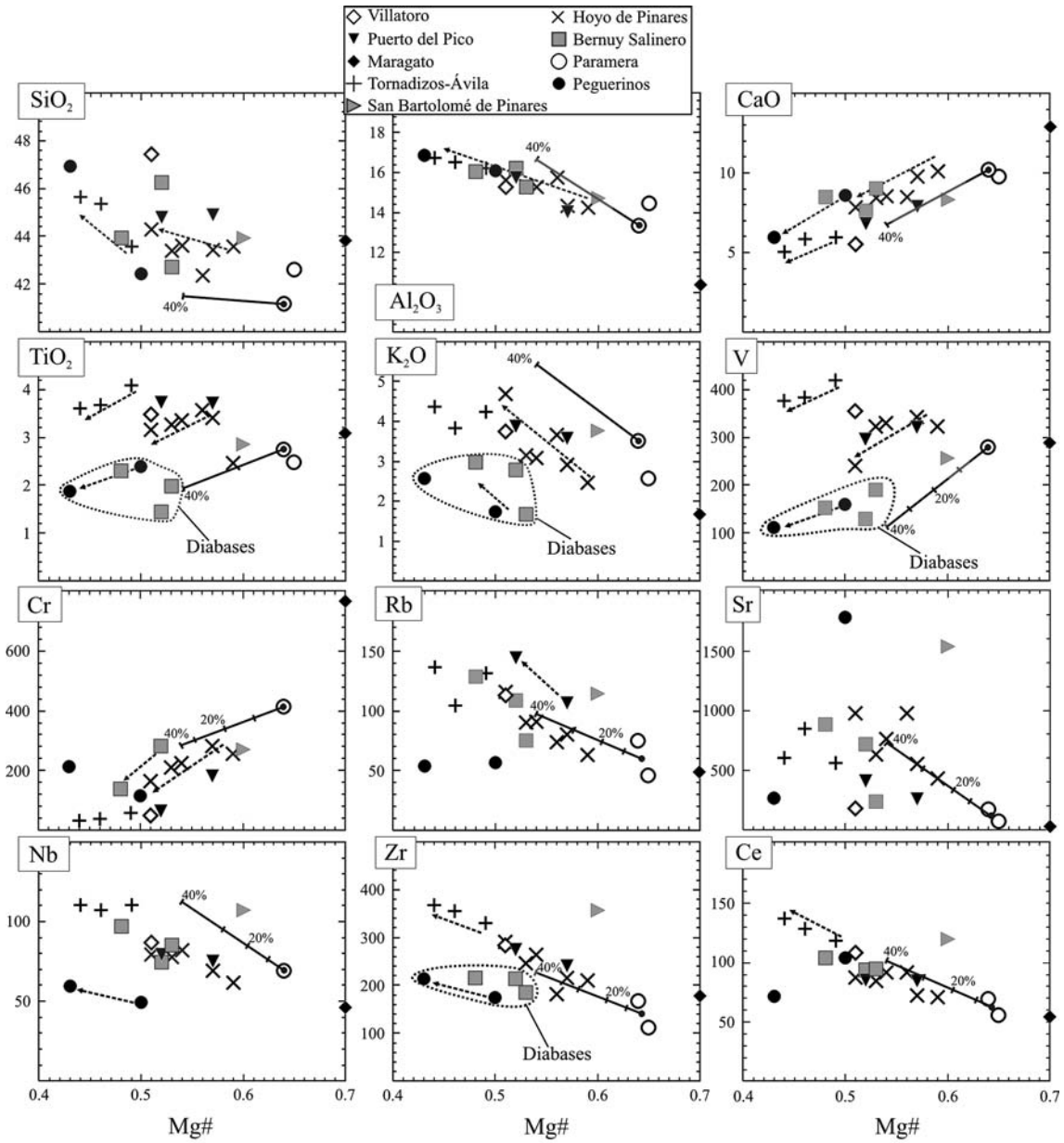

Fig. 5 Major and trace element composition of the SCS alkaline basic dykes. Concentrations expressed as weight % (SiO_2, Al_2O_3, CaO, TiO_2 and K_2O) and ppm (V, Cr, Rb, Sr, Nb, Zr and Ce). The *black arrows* indicate the compositional variation trend observed within samples from a single dyke. The *solid grey line* displays the output data of a fractional crystallization model applied on major and trace elements and made on the basis of the general Rayleight equation. The model input data consider fractionation of 20% cpx, 7% ol and 13% amph, obtained by averaging phenocrysts modal proportions. Clinopyroxene 103811-62, amphibole 80318-9 and olivine 104867-57 from Tables 1 and 2 have been used in major element modeling. As initial magma composition we have considered the most Mg-rich non cumulate samples from La Paramera dyke (76547 and 77753). Mineral/melt partition coefficients for clinopyroxene, olivine and amphibole used for modeling trace elements (except Cr, V) taken, respectively, from Foley et al. (1996), Zanetti et al. (2004) (except Nb after Taura et al. 1998) and LaTourrette et al. (1995). $D_{Cr}^{Cpx/melt}$, $D_{V}^{Cpx/melt}$ and $D_{Cr}^{Ol/melt}$ after Ringwood (1970); $D_{V}^{Amph/melt}$ and $D_{V}^{Ol/melt}$ after Dostal et al. (1983) and $D_{Cr}^{Amph/melt}$ after Matsui et al. (1977)

differences to be due to a significant mantle compositional effect. This is discussed below.

Spanish Central System alkaline rocks do not show primary magma compositions according to the criteria of Frey et al. (1978): Mg# > 0.6–0.7; Cr > 500–1,000 ppm and Ni > 200–500 ppm (Table 3). Moreover, the forsterite content of olivines from primary magmas are normally in the range 88–94, whilst olivines from SCS lamprophyres and diabases do not exceed Fo_{86}, suggesting the involvement of one or more differentiation processes. Of particular interest is the alkaline dyke from Maragato, which shows the richest composition in Mg, Cr and Ni (Fig. 5). These

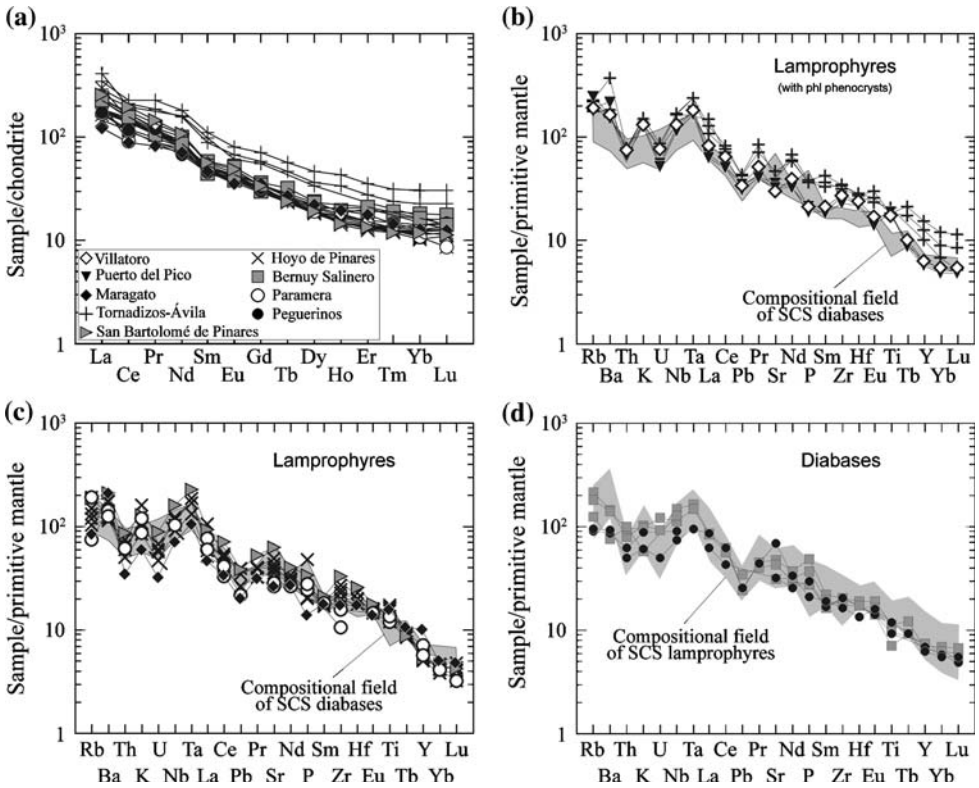

Fig. 6 **a** Chondrite-normalised and **b, c** and **d** primitive mantle-normalised trace element composition of the SCS alkaline basic dykes. Lamprophyres containing phlogopite phenocrysts and diabasic samples have been plotted separately for trace element spidergrams, whereas they all have been plotted together for REE. The normalising values of chondrite and primitive mantle are after Sun and McDonough (1989) and McDonough and Sun (1995), respectively

contents are probably influenced by the cumulative nature of this dyke, as deduced from its high proportion (>40%) of mafic phenocrysts (mainly clinopyroxene and pseudomorphosed olivine).

The positive correlation of Ca, Ni, Cr and V versus Mg# value points to ol + Cr-sp + cpx crystal fractionation. Additionally, the trends of Ti depletion observed in Fig. 5 are likely to be due to kaersutite fractionation. These premises are consistent with the petrographic observations. We have applied a crystal fractionation model based on major and trace elements for the lamprophyric melts; the results are plotted in Fig. 5. A 40% fractionation of cpx + amph + ol is enough to account for the compositional trends observed in the SCS lamprophyric magmas (more details in caption to Fig. 5). This model should be considered as a general indication of the fractionation process followed by the different alkaline dyke swarms (e.g. for diabasic magmas a different crystal fractionation process involving plagioclase should be considered).

Role of crustal assimilation

The entrapment of granulite and cumulate ultramafic xenoliths whose estimated pressure of equilibration ranges from 7 to 12 kbar (Villaseca et al. 1999; Orejana et al. 2006) seems to indicate that the SCS lamprophyric and diabasic melts might have stagnated at lower crustal levels. This is reinforced by the fact that some of those ultramafic cumulate xenoliths are genetically related with the Permian alkaline magmatism (Orejana et al. 2006), and also because some lamprophyres carry a complex high-pressure phenocryst population (Orejana et al. 2007). Thus, the question of a possible lower crustal contamination process arises. Ratios of trace elements with contrasting concentrations in mantle and crustal rocks may help to evaluate this possible influence. Ce/Pb and Ba/Nb ratios in the continental crust are around 3.9 and 57, respectively (Rudnick and Gao 2003) due to the high Pb and Ba concentrations in the crust. These values are close to those of the SCS granulite xenoliths from the lower crust (Ce/Pb ~5 and Ba/Nb ~66; Villaseca et al. 1999). The same ratios in the SCS alkaline lamprophyres and diabases are significantly different (Ce/Pb = 14–28 and Ba/Nb = 9–15), approaching the trace element composition of typical mantle-derived rocks (OIB: Ce/Pb ~25 and Ba/Nb ~7.3; Sun and McDonough 1989) (Fig. 9a). Three SCS lamprophyres show Ba/Nb from 15 to 29, although these high values are probably derived from the high proportions of phlogopite (Ba-rich) and clinopyroxene (Nb-poor) phenocrysts.

We have tested an AFC model using Ce/Pb and Ba/Nb ratios to quantify the degree of assimilation of lower crustal materials on the composition of the SCS alkaline dykes (see input data in Fig. 9 caption). The results shown in Fig. 9a are based on three different assimilation/fractionation (r) values. Leaving aside the three samples with high Ba/Nb discussed above, the small compositional differences

Table 4 Sr–Nd–Pb Isotopic composition of SCS alkaline lamprophyres and diabases

	Lamprophyres						Diabases		
Dyke	Paramera	Tornadizos-Ávila	Hoyo de Pinares	Maragato	Puerto del Pico	San Bartolomé de Pinares	Bernuy Salinero	Peguerinos	Peguerinos
Sample	77753[a]	103473[a]	103674[a]	103811	103818	104541[b]	81839[b]	81938[a]	101892[b]
Rb (ppm)	74	137	91.4	48.9	107	115	129	54	56.5
Sr (ppm)	429	803	880	514	631	1266	942	633	1387
$^{87}Rb/^{86}Sr$	0.50	0.49	0.30	0.28	0.49	0.26	0.40	0.25	0.12
$^{87}Sr/^{86}Sr \pm (2\sigma)$	0.704850 ± 03	0.706246 ± 06	0.705803 ± 05	0.706147 ± 32	0.707004 ± 23	0.705798 ± 07	0.705276 ± 12	0.704455 ± 06	0.703741 ± 08
$^{87}Sr/^{86}Sr_{265\ Ma}$	0.70297	0.70438	0.70467	0.70511	0.70515	0.70481	0.70378	0.70352	0.70330
Sm (ppm)	7.12	16.9	7.45	7.07	7.37	8.69	8.91	6.91	7.65
Nd (ppm)	35.2	84.4	42.9	33.2	39.6	50.9	46.5	31.68	42.2
$^{147}Sm/^{144}Nd$	0.122	0.121	0.105	0.129	0.113	0.103	0.116	0.132	0.110
$^{143}Nd/^{144}Nd \pm (2\sigma)$	0.512841 ± 08	0.512465 ± 03	0.512551 ± 04	0.512523 ± 05	0.512444 ± 06	0.512500 ± 06	0.512860 ± 10	0.512728 ± 03	0.512832 ± 05
$e(Nd)_{265\ Ma}$	6.5	−0.8	1.4	0.1	−0.9	0.5	7.1	4.0	6.7
U (ppm)	1.32	1.75	1.19		1.03	1.82	1.87		1.02
Th (ppm)	5.00	6.21	5.26		5.17	6.94	6.42		4.01
Pb (ppm)	3.28	6.56	5.47		4.67	6.09	3.65		4.56
$^{238}U/^{204}Pb$	30.0	19.4	17.0		17.2	22.8	37.4		17.0
$^{232}Th/^{204}Pb$	125.0	69.0	75.1		86.2	86.8	128.4		66.8
$^{206}Pb/^{204}Pb \pm (2\sigma)$	19.548 ± 0.006	19.281 ± 0.004	19.047 ± 0.020		19.129 ± 0.010	19.411 ± 0.010	19.808 ± 0.040		19.225 ± 0.014
$^{207}Pb/^{204}Pb \pm (2\sigma)$	15.675 ± 0.006	15.617 ± 0.004	15.640 ± 0.020		15.680 ± 0.010	15.649 ± 0.010	15.629 ± 0.040		15.624 ± 0.012
$^{208}Pb/^{204}Pb \pm (2\sigma)$	39.658 ± 0.006	39.268 ± 0.004	39.211 ± 0.020		39.582 ± 0.010	39.553 ± 0.010	39.632 ± 0.040		39.180 ± 0.014
$^{206}Pb/^{204}Pb_{(265\ Ma)}$	18.163	18.465	18.334		18.409	18.456	18.239		18.512
$^{207}Pb/^{204}Pb_{(265\ Ma)}$	15.604	15.575	15.603		15.643	15.600	15.548		15.587
$^{208}Pb/^{204}Pb_{(265\ Ma)}$	38.008	38.357	38.219		38.445	38.408	37.937		38.298

Rb, Sr, Sm, Nd, U, Th and Pb concentrations determined by ICP-MS

[a] Sr–Nd isotopic data of these samples taken from Villaseca et al. (2004)

[b] Sr–Nd isotopic data of these samples taken from Orejana et al. (2006)

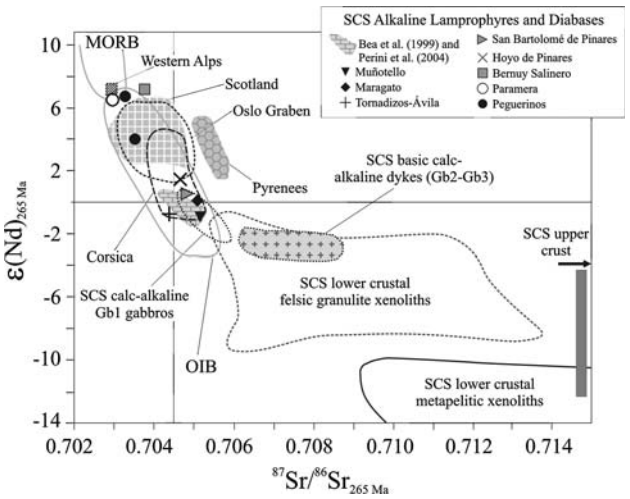

Fig. 7 Sr–Nd isotopic composition of the SCS alkaline basic dykes compared with that of other alkaline or moderately alkaline Permian basic rocks from western Europe, including previous analyses of Bea et al. (1999) and Perini et al. (2004) for the SCS alkaline lamprophyres. Maragato and Puerto del Pico samples represent new data, whilst the rest of plotted samples are taken from Villaseca et al. (2004) and Orejana et al. (2006). Compositional field of Pyrenees, Oslo Graben, Scotland, Corsica and Western Alps are taken from Lago et al. (2004), Neumann et al. (2004), Upton et al. (2004), Bonin (2004) and Monjoie (2004), respectively. It has been also plotted for comparison the composition of the Gb1 and Gb2–Gb3 calc-alkaline post-collisional dykes from the SCS, after Villaseca et al. (2004). The isotopic signatures of the SCS lower crustal felsic granulite xenoliths and metapelitic xenoliths are taken from Villaseca et al. (1999). SCS upper crustal materials (*grey vertical bar*) plot mostly out of the diagram, towards much higher $^{87}Sr/^{86}Sr$ values (Villaseca et al. 1998b). OIB and MORB fields after Wilson (1989)

displayed by the SCS alkaline dykes would require no more than 7% assimilation of lower crustal rocks. Moreover, there is not a positive correlation of silica content with Sr isotope radiogenic ratios or Rb/Sr values in these alkaline rocks (Fig. 9b,c), as would be expected if a silica-rich crustal component were involved in their genesis. Additionally, the negative Pb anomalies and Nb–Ta peaks shown by the SCS alkaline dykes when normalized to primitive mantle contents (Fig. 6), support the contention that contamination by lower crustal rocks did not exert a significant influence on their composition.

Source enrichment and mantle heterogeneity

The primitive mantle-normalised Sm/Yb ratios in the SCS alkaline basic rocks range from 2.4 to 5.3, and these values are consistent with melting in the presence of residual garnet (e.g. McKenzie and O'Nions 1991). Furthermore, their high incompatible trace element contents probably indicate the involvement of an enrichment process in the mantle source.

Th/Yb and Ta/Yb ratios in basic rocks are a useful petrogenetic indicator. In Fig. 10a we have represented the

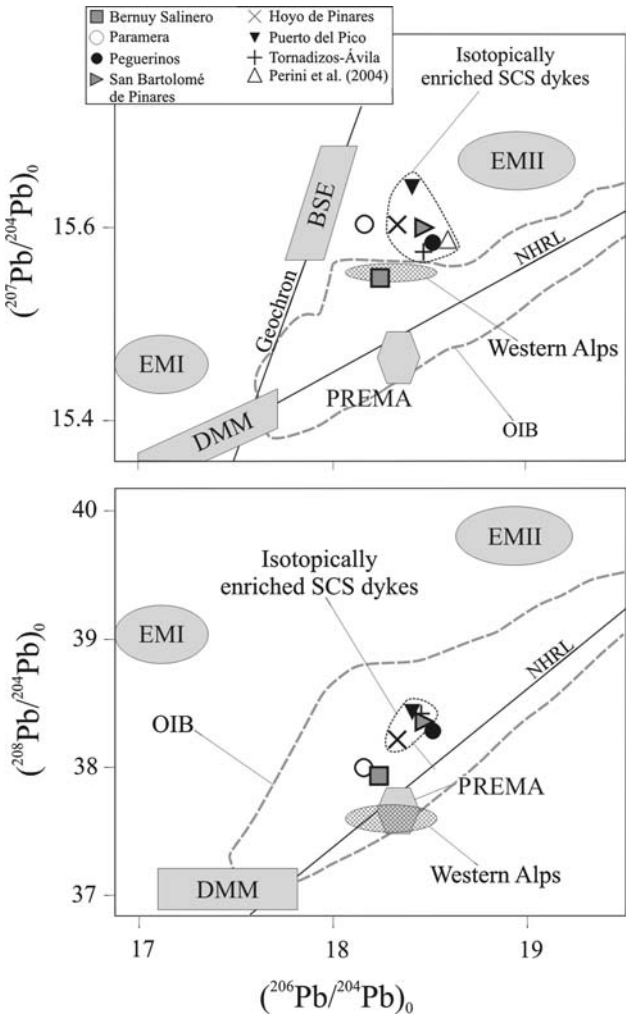

Fig. 8 Pb isotope ratios of the SCS alkaline basic dykes. The single data of Perini et al. (2004) corresponds with a single SCS alkaline lamprophyre. It has also been plotted for comparison the compositional field of the Permian moderately alkaline dykes from western Alps (Monjoie 2004). Compositional fields of OIB, DMM, BSE, EMI, EMII, PREMA and HIMU are taken from Zindler and Hart (1986). NHRL: Northern Hemisphere Reference Line

compositional fields of mantle-derived rocks from depleted and enriched sources (following the mantle array) and those of island arc basalts (IAB) and active continental margins (taken after Wilson 1989). The involvement of crustal rocks or subduction components in IAB and continental margins is reflected in their Th enrichment and Ta depletion with respect to REE. The SCS alkaline basic dykes plot within the mantle array and completely overlap the enriched field of mantle rocks, with a composition similar to OIB (Fig. 10a), thus supporting a minor contribution of crustal assimilation and suggesting that primary magmas of these rocks were generated by partial melting of a metasomatised mantle.

For SCS alkaline lamprophyres there are positive correlations between Rb/La and K/La ratios, and also between

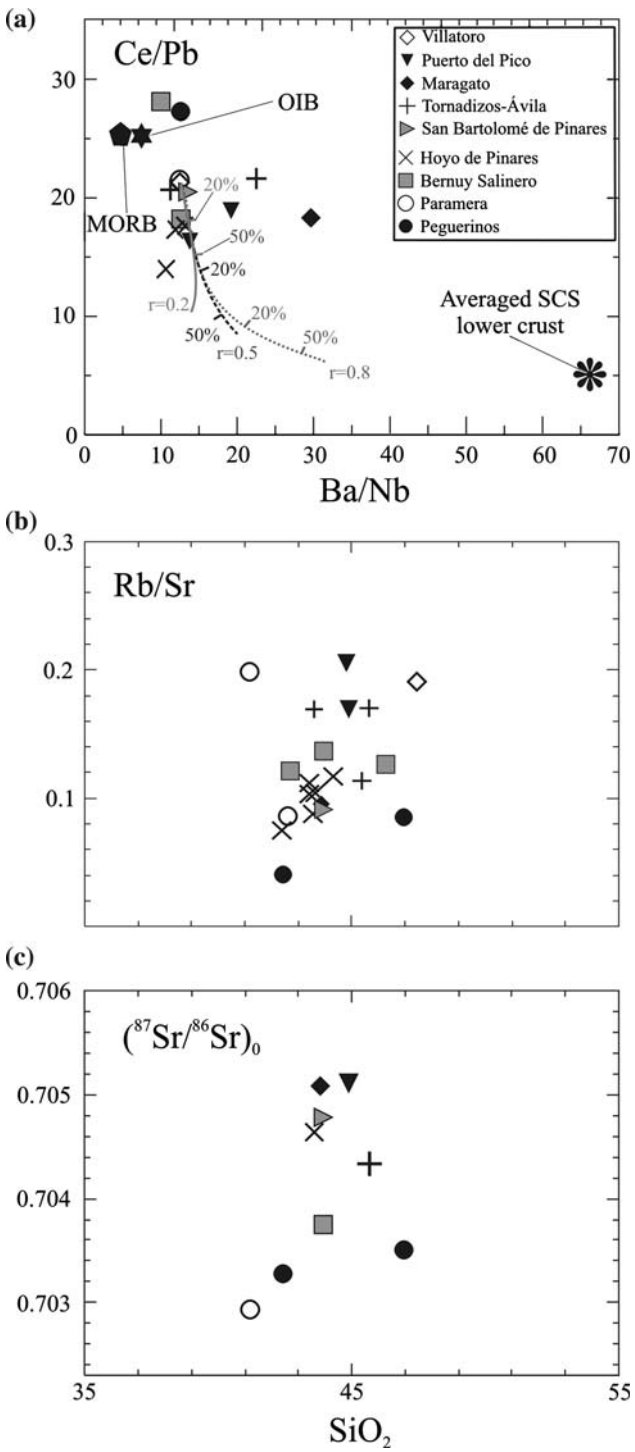

Fig. 9 Whole-rock chemical composition of SCS alkaline basic dykes for **a** Ce/Pb versus Ba/Nb, **b** SiO_2 versus Rb/Sr and **c** SiO_2 versus $(^{87}Sr/^{86}Sr.)_0$. Plot (**a**) also shows an AFC model made for three contrasting assimilation/fractionation ratios (0.2, 0.5 and 0.8). Initial model melt composition: sample 77753 (La Paramera dyke). Contaminant composition: averaged values of SCS lower crustal granulite xenoliths (Villaseca et al. 1999). The bulk D_{Nb} (0.06), D_{Ba} (0.05), D_{Ce} (0.07) and D_{Pb} (0.03) have been calculated using the mineral/melt partition coefficients and the proportions of fractionating phases described in Fig. 5 caption, with the exception of D_{Pb}, for which ol/melt and amph/melt partition coefficients have been taken from McKenzie and O'Nions (1991). MORB and OIB average composition in diagram (**a**) are taken from Sun and McDonough (1989)

Ba/Nb and Ba/Ce ratios (Fig. 10b, c). These features might account for the presence of phlogopite in the source during partial melting as this mineral may preferentially incorporate LILE when compared to REE and HFSE. This is also supported by the potassic character of lamprophyres; potassic and ultrapotassic rocks are associated with the presence of phlogopite in the mantle (e.g. Foley 1992). The high Nb–Ta concentrations observed in the SCS alkaline dykes (Table 3) suggest that pargasitic amphibole has also participated in their genesis controlling the behavior of Nb–Ta during mantle melting (e.g. Ionov et al. 1997). Moreover, the SCS diabases have higher Nb/Ta ratios (13.6–16.1) when compared to the lamprophyres (11.2–13.1). Green (1995) found that pargasite is the only mineral involved in the genesis of basaltic magmas that shows $D_{Nb/Ta} > 1$, and thus the melt Nb/Ta ratio is controlled by amphibole during melting (Tiepolo et al. 2000). Therefore, although both potassic phases might have coexisted, amphibole was probably predominant in the mantle sources of SCS diabases, whilst the influence of phlogopite is evident mainly in the case of lamprophyres. The moderate P_2O_5 content of the SCS alkaline dykes (0.3–1 wt%; Table 3) indicate that a P-rich phase, such as apatite, might have been a stable metasomatic mineral in the mantle source. Slight negative P anomalies can be observed in these dykes (Fig. 6) indicating the presence of a residual P-rich mineral in the mantle. Samples showing positive P anomalies are those characterized by high proportions of accumulated apatite phenocrysts (e.g. sample 81839).

A diabase-lamprophyre association within the Permo-Carboniferous magmatism in western Europe has also been reported in southern Scandinavia by Obst et al (2004). Nevertheless, these diabases are tholeiitic in composition and they are derived from a depleted mantle source subjected to a metasomatic event that is genetically unrelated to the coeval alkaline lamprophyres. On the contrary, the SCS diabase-lamprophyre association consists of similar alkaline magma batches (e.g. Fig. 6), which also overlap in their Sr–Nd–Pb isotopic compositional fields, suggesting that they are derived from similar mantle sources with only slight differences in their modal accessory mineralogy.

The isotopic composition of the SCS alkaline magmas implies the involvement of at least two different mantle sources: one isotopically depleted (PREMA-like) and the other isotopically enriched. The depleted Sr–Nd isotope signatures of diabases and some lamprophyres indicate participation of a sublithospheric source (probably asthenosphere-related). However, the lamprophyres with more radiogenic Sr–Nd isotopic compositions clearly

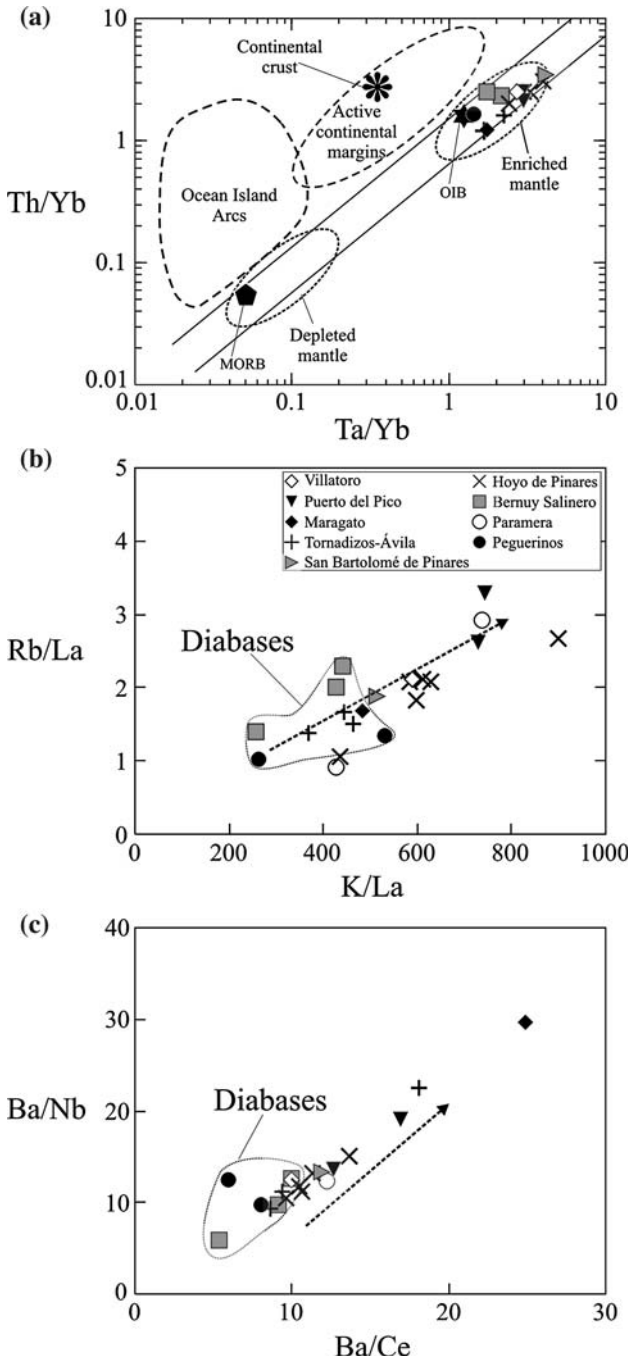

Fig. 10 Whole-rock chemical composition of SCS alkaline basic dykes for **a** Th/Yb versus Ta/Yb, **b** Rb/La versus K/La and **c** Ba/Nb versus Ba/Ce. *Arrows* represent the general trend described by the SCS alkaline dykes. MORB and OIB average composition in diagram (**a**) are taken from Sun and McDonough (1989), and Continental crust average composition taken from Rudnick and Gao (2003). The fields of Oceanic Island Arcs and Active Continental Margins after Wilson (1989)

indicate the involvement of a lithospheric mantle. Metasomatism of both asthenospheric and lithospheric mantle sources is likely to have acted in a similar way, producing the same enrichment patterns; the highly incompatible trace element ratios in both lamprophyres and diabases are not significantly different (e.g. Fig. 10a).

Mantle metasomatism has been attributed to either (1) fluids or melts generated by subduction processes (e.g. Peacock 1990), or (2) volatile- and K-rich, low-viscosity melts that leak from the asthenosphere and accumulate in the overlying lithosphere (e.g. McKenzie 1989). The composition of these agents is believed to change continuously as they percolate thorough the mantle from their source regions (Navon and Stolper 1987). Normalised multi-element plots (Fig. 6) for the SCS alkaline basic dykes do not have subduction-related signatures, such as large negative Nb, Ta and Ti anomalies, and thus we attribute the source enrichment to metasomatising melts derived from the convecting mantle. McKenzie (1989) suggested that these melts would freeze in the lithosphere and might concentrate in thin zones over long periods of time, resulting in substantial volumes accumulated as veins, sills or dykes in a mechanical boundary layer. Melting of this metasomatised mantle might lead to the generation of potassic–ultrapotassic rocks (e.g. Chalapathi Rao et al. 2004). The potassic nature of the SCS alkaline lamprophyres is in accordance with this latter model.

The involvement of a continental component in the SCS lamprophyre mantle sources is difficult to assess. The Sr–Pb isotopic signatures of the enriched lamprophyres are indicative of the introduction of a ^{87}Sr–^{207}Pb–^{208}Pb-rich component into the mantle. These characteristics cannot be explained by the generation of phlogopite in mantle sources during the metasomatic event. This mineral usually displays high Rb/Sr and low U/Pb ratios, thus an enrichment in radiogenic Pb would not be expected. Furthermore, the high Rb-REE concentrations in the isotopically depleted dykes argue against extended evolution of the mantle sources after being metasomatised. We consider that the ^{207}Pb–^{208}Pb-rich composition of these rocks could be derived from a component similar to the reservoir EMII, which could be related to the incorporation of continental crust into the mantle (Zindler and Hart 1986). The subcontinental lithospheric mantle source of these lamprophyres has been slightly modified by subducted crustal components, now only detectable because of their isotopic signatures. But the origin and age of this metasomatic event is difficult to establish with the current data.

The geodynamic context of the SCS alkaline magmatism within the Permian magmatic province of western Europe

The intrusion of the SCS alkaline magmas is considered to be part of the widespread magmatism developed in western Europe at the end of the Hercynian orogeny, with extensive

alkaline magmatic manifestations from the northern foreland to the internal zones (Wilson et al. 2004 and references therein). In Fig. 11 we have highlighted the location of the most important Permian basic magmatic regions in western Europe, together with the main structural lineations that were active at that time (see references in Fig. 11 caption). According to different studies, this Permian magmatism coincided with a period of incipient regional rifting (Bonin 1988; Ziegler 1993; Heeremans et al. 2004). Nevertheless, a palaeomagnetic study on Permian volcanic rocks from the western Alps has shown that a single geodynamic setting might not be applicable to the whole area (Muttoni et al. 2003). These authors propose that part of the S-Europe region would have been assembled with Africa (Gondwana) during Early Permian times. This is in agreement with the model of Irving (1977), which suggests that a significant change might have occurred in the palaeogeographic configuration of the Pangea supercontinent from early to late Permian, placing Gondwana farther to the East by approximately 3,000 km with respect to Laurasia at the beginning of this period. This transition from Pangea 'B' to Pangea 'A' has been associated with an intraplate dextral megashear system and with the reactivation of Hercynian shear zones (Muttoni et al. 2003). The Hercynian front could be related to one of these megashear bands.

Figure 12 shows the time intervals of Permian basic magmatism as a function of magmatic affinity (calc-alkaline, alkaline and tholeiitic) within western Europe. Calc-alkaline rocks are clearly confined to lower Permian or older ages within SW Europe and do not coexist with alkaline intrusions in the internal zone of the orogen, with the exception of Corsica-Sardinia (Cocherie et al. 2005) (Fig. 12). Additionally, Carboniferous alkaline rocks are confined to NW Europe. In Scotland this magmatism starts in the Dinantian (from 342 ± 1 Ma; Monaghan and Pringle 2004) and persists during Permian times (Upton et al. 2004; Kirstein et al. 2006). Something similar is observed in the Oslo Graben, where alkaline basalts were intruded between 305 and 299 Ma and larvikitic and basanite lavas follow in several stages until 243 Ma (Neumann et al. 2004). Highly alkaline basalts and basanites are characteristic of the lower Permian

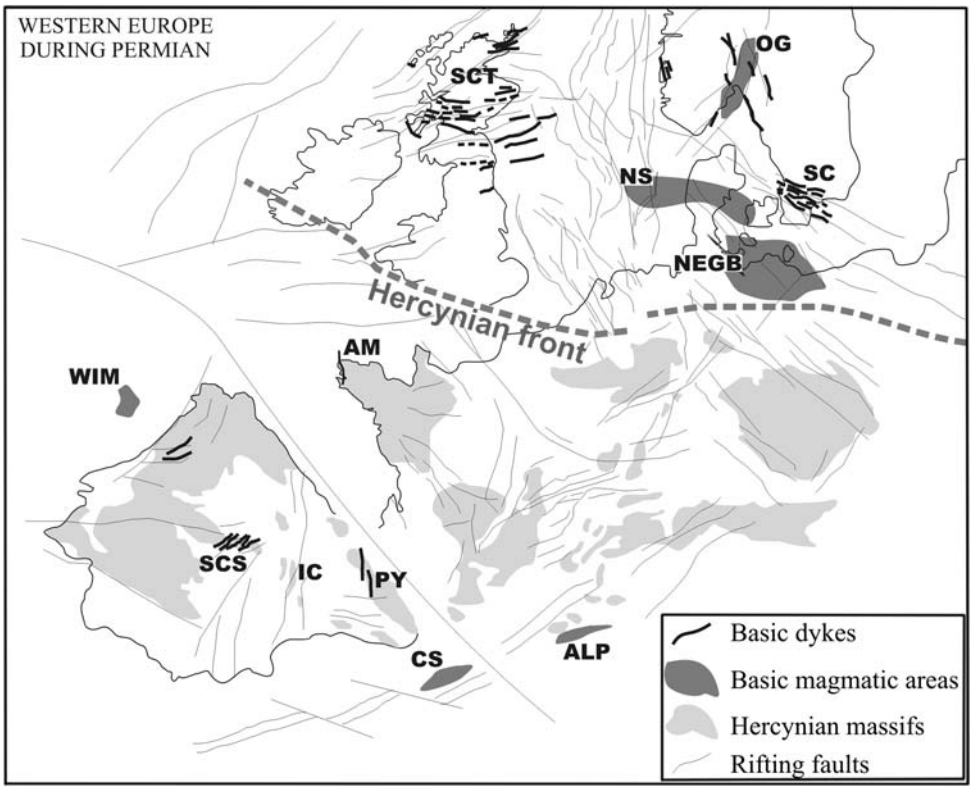

Fig. 11 Sketchy map made after Franke (1989) showing the location of the main magmatic regions within western Europe during Permian. *WIM* West Iberian Margin, after Gardien and Paquette (2004); *P* Portugal, after Portugal-Ferreira and Macedo (1977); *PY* Pyrenees, after Debon and Zimmermann (1993) and Lago et al. (2004); *IC* Iberian Chain, after Lago et al. (2005); *AM* Armorican Massif, after Bellon et al. (1988); *CS* Corsica-Sardinia, after Bonin (1988); *ALP* western and southern Alps, after Cortesogno et al. (1998) and Rottura et al. (1998); *SCT* Scotland, after Upton et al. (2004); *NS* North Sea, after Heeremans et al. (2004) and Stemmerik et al. (2000); *NEGB* North East German Basin, after Neumann et al. (2004), *OG* Oslo Graben, after Neumann et al. (2004) and *SC* Scania, after Neumann et al. (2004). Structural lineations after Bonin (1988), Ziegler (1993), Heeremans et al. (2004) and Ziegler et al. (2004). Hercynian front after Kirstein et al. (2006)

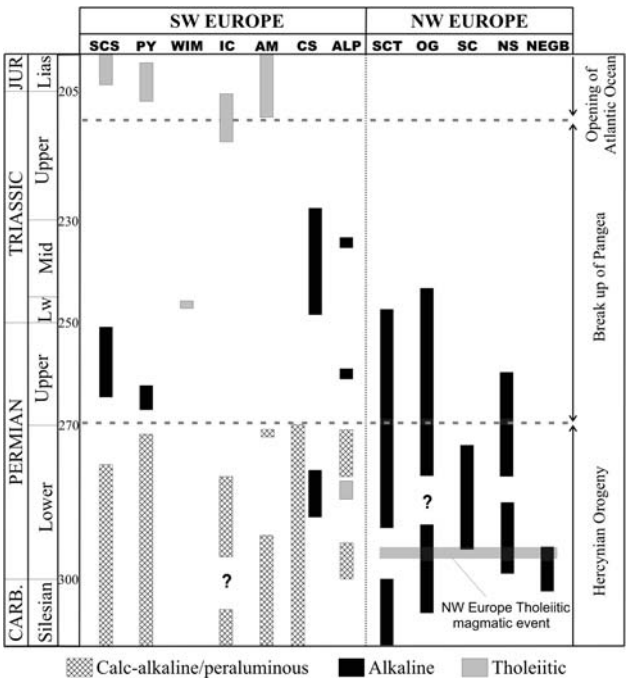

Fig. 12 Chronology of the main Permian-Triassic basic magmatism in western Europe. *PY* Pyrenees, after Alibert (1985), Debon and Zimmermann (1993) and Lago et al. (2004); *WIM* West Iberian Margin, after Gardien and Paquette (2004); *IC* Iberian Chain, after Lago et al. (2005); *AM* Armorican Massif, after Bernard-Griffiths et al. (1985) and Bellon et al. (1988); *CS* Corsica-Sardinia, after Traversa et al. (2003), Bonin (2004) and Cocherie et al. (2005); *ALP* western and southern Alps, after Rottura et al. (1998), Eichhorn et al. (2000), Carraro and Visonà (2003) and Monjoie (2004); *SCT* Scotland, after Upton et al. (2004); *NS* North Sea, after Stemmerik et al. (2000); *NEGB* North East German Basin, *OG* Oslo Graben and *SC* Scania, after Neumann et al. (2004). NW Europe tholeiitic magmatic event at 295 Ma are taken from Heeremans et al. (2004)

in Scania (294–274 Ma) and the NE German basin (294–302 Ma) (Neumann et al. 2004). A similar age range has been obtained for basic volcanics (strongly alkaline basalts and basanites) from the North Sea basins (broadly 299–260 Ma; Stemmerik et al. 2000; Neumann et al. 2004). Minor tholeiitic volcanics may accompany the more abundant alkaline rocks in NW Europe Permo-Carboniferous regions. Moreover, a regional tholeiitic magmatic event recorded around 295 Ma characterizes these northern areas (Heeremans et al. 2004), but was not seen in SW Europe (Fig. 12). On the other hand, tholeiitic magmas occur in SW Europe in continental areas at the Triassic–Jurassic boundary, as exemplified by the SCS and Pyrenees intrusions.

Accordingly, a geochemical contrast exists when comparing SW and NW Europe basic magmatism during the Permian. In SW Europe tholeiitic and alkaline magmatism is mostly absent during the Lower Permian (excepting Corsica-Sardinia; Fig. 12), whereas calc-alkaline magmatism is dominant and it does not appear in NW Europe. This discrepancy supports the possibility outlined by Muttoni et al. (2003), that NW and SW Europe were geographically farther apart during the Early Permian than previously thought. The widespread alkaline magmatic event recorded in both SW and NW Europe (SCS, PY, CS, ALP, SCT, OG, SC, NS and NEGB) during the Mid Permian might represent the assembly of all western Europe, to configure Pangea 'A' within the framework of a common general geodynamic setting.

In the SCS, the intrusion of the alkaline suite during Upper Permian marks the change from the last Hercynian extensional stages to widespread post-Hercynian rifting. This latter global faulting might represent the break up of Pangea, but it has also been linked to the opening of the Atlantic Ocean and the development of the Central Atlantic Magmatic Province (Bonin 1988). This latter possibility could be supported by the alkaline-tholeiitic transition during the Upper Triassic. This mainly occurs near ocean margin regions (the ocean–continent transition zone in the NW of the Iberian Massif and Armorican Massif; Fig. 12).

The marked change in the geochemical composition of the magmatism from Lower to Upper Permian in SW Europe, means the introduction of deeper mantle-derived melts with isotopically depleted components, as evidenced by their positive ε(Nd) values (Corsica, Bonin 2004; western Alps, Monjoie 2004; Pyrenees, Lago et al. 2004, and the SCS) (Fig. 7). Although this new isotopic signature is also recorded in NW Europe (Oslo Graben, Neumann et al. 2004; Scotland, Upton et al. 2004), it appears as early as 342 $\pm$ 1 Ma in Scotland (Monaghan and Pringle 2004), indicating a different geological history for this northern sector when compared to southern Europe, reinforcing the geodynamic hypothesis proposed above.

Permian alkaline melts from the SW Europe (e.g. Corsica-Sardinia, SCS area) display magma types with lower εNd values than NW Europe alkaline regions, plotting close to BSE (Fig. 7). Thus, an enriched lithospheric mantle component has been involved in the genesis of alkaline magmas in those southern European areas (e.g. Perini et al. 2004). This is in agreement with Pb isotope data, as discussed in the previous section. Nevertheless, Upper Permian alkaline magmatism in western Europe is considered to be mainly derived from mantle sources without the involvement of significant subduction-contaminated components (Wilson et al. 2004). Intracontinental rifting at the end of the Hercynian orogeny within central–western Europe has been suggested, implying lithosphere thinning and ascent of hot deep mantle (Wilson et al. 2004 and references therein). Four possible mechanisms may account for this general process of rifting and associated mantle melting: (1) breakoff of a subducting slab; (2) delamination of the lower crust; (3) impingement of a mantle plume; and (4) passive upwelling of

asthenosphere as continental fragments diverge and melting occurs by adiabatic decompression.

Models involving crustal sinking (slab breakoff or lower crustal delamination) are unlikely due to the absence of significant subduction-related components in the SCS lithospheric mantle sources.

The origin of the Permo-Carboniferous volcanic province in Europe and NW Africa has been interpreted in terms of a superplume impinging on the base of the lithosphere (Ernst and Buchan 1997). According to this model, the head of this superplume would have spread northward asymmetrically from the incipient Atlantic rift (Oyarzun et al. 1997; Wilson 1997), covering a roughly elliptical area of 4,000 km from Morocco to the Oslo Graben. Its influence in western Europe is speculated to continue during Mesozoic and Cenozoic times and is further related to the opening of the Atlantic Ocean (e.g. Burke et al. 1973; White and McKenzie 1989; Oyarzun et al. 1997). The small magma volumes represented by these alkaline dykes and the absence of magmatism between 252 ± 3 Ma (the youngest age determined for the SCS alkaline suite; Fernández Suárez et al. 2006) and 203 ± 2 Ma (intrusion of the tholeiitic Messejana-Plasencia dyke; Dunn et al. 1998) in central Spain, contradicts the classical theory of a deep mantle plume, continuously generating large magma volumes over a long period of time (Campbell 2005 and references therein). Moreover, no anomalously thick crust due to igneous accretion (underplating) of mafic rocks is known to have existed beneath the SCS. In fact, the composition of the lower crust seems to be felsic as indicated by the granulite xenoliths carried by the alkaline dykes (Villaseca et al. 1999). Recently, based on the absence of large magma volumes, thermal anomalies and low $^{3}He/^{4}He$ ratios, Kirstein et al. (2004) found no compelling evidence of mantle plume involvement in the genesis of Permo-Carboniferous magmatism in NW Europe. This criticism with the plume model has also been extended to the opening of the central Atlantic Ocean (McHone 2000).

We suggest that the most probable geodynamic setting for the generation of the SCS alkaline magmas is that of lithosphere thinning, passive upwelling of hot asphenospheric mantle and melting forced by adiabatic decompression. Asthenosphere-like melts might be identified with the isotopically depleted SCS dykes, whilst the lamprophyres with BSE-like isotopic compositions are recording melting at the base of the lithosphere. The present lithospheric thickness in central Spain is around 110 km (Fernández et al. 1998; Tejero and Ruiz 2002) and the region seems to have been tectonically stable since Permian times. Moreover, alkaline melt generation occurred at great depth (the stability field of garnet in peridotites ranges down to around 80 km; Nickel 1986) close to the proposed lithosphere–asthenosphere boundary. The occurrence of alkaline mafic dykes in the western Alps at 260 ± 1 Ma (Monjoie 2004) has also been ascribed to melting of an asthenosphere-like mantle as a consequence of lithosphere thinning. The close similarities, which exist in the geochronology and isotope geochemistry of the alkaline magmas from the SCS, Pyrenees and western Alps support the regional scale extension of this geodynamic context in southern Europe during the Permian.

Summary and conclusions

The alkaline lamprophyres and diabases from the SCS constitute a petrographically and geochemically heterogeneous suite of dykes. The abundance of mafic phenocrysts, the absence of primary magmas and presence of variation trends characterized by decreasing Ca, Ti, Ni, Cr and V towards lower Mg#, is in accordance with fractionation of olivine + clinopyroxene + kaersutite ± Cr-spinel ± ulvospinel ± plagioclase (this latter mineral only in the case of diabases).

Their bulk chemistry has not been influenced significantly by assimilation of crustal rocks, as their incompatible trace element ratios are similar to those of rocks typically derived from mantle sources (Ce/Pb and Ba/Nb in OIB and MORB). Moreover, they do not show positive correlation of silica content with Rb/Sr or $^{87}Sr/^{86}Sr$ ratios.

The clear positive Nb–Ta and negative Pb anomalies indicate that enrichment of their sources was not caused by any subduction-related component. The highly fractionated chondrite-normalised REE patterns and high Sm/Yb_N ratios suggest that they formed within the garnet stability field. The potassic nature of the SCS lamprophyres and their Rb/La and K/La ratios point to phlogopite dominating their generation, whereas amphibole prevailed in the case of the sodic diabases. It is likely that the enrichment event was caused by infiltration of K- and volatile-rich fluids or melts. The high REE contents shown by the isotopically depleted dykes imply that melting occurred shortly after metasomatism.

Two isotopic groups of SCS alkaline dykes are observed: (1) a PREMA-like (asthenosphere) component ($\varepsilon Nd = +4$ to $+7.1$; $^{87}Sr/^{86}Sr = 0.7029–0.7037$; $^{206}Pb/^{204}Pb = 18.1–18.5$); and (2) a BSE-like or slightly enriched lithospheric component ($\varepsilon Nd = +1.4$ to -0.9; $^{87}Sr/^{86}Sr = 0.7043–0.7051$; $^{206}Pb/^{204}Pb = 18.3–18.5$). The slight enrichment in ^{87}Sr, ^{207}Pb and ^{208}Pb isotope ratios can be ascribed to the introduction into the mantle sources of continental or subduction-modified components.

A clear geochemical contrast can be observed when comparing lower Permian basic magmatism from SW and NW Europe. In areas north of the Hercynian front, no

calc-alkaline or peraluminous magmatism is recorded at that time and alkaline manifestations are widespread. In areas affected by the Hercynian orogeny alkaline magmas are scarce before Upper Permian times. Moreover, northern areas show a regional tholeiitic event around 295 Ma, which does not exist in SW Europe. This difference agrees with the model outlined by Muttoni et al. (2003) in which NW and SW Europe were geographically assembled during mid Permian times.

Though a mantle plume has been proposed as the principal factor responsible for the rifting process during Permo-Carboniferous times there are features that are not in accordance with this model when applied to the SCS. This has also been argued for the magmatism in Northern Europe (e.g. Kirstein et al. 2004, 2006). Thus we favor a passive model in which rifting would follow from lithosphere thinning and upwelling of the hot asthenosphere. This tectonic regime might be transitional between the general Permo-Carboniferous extension in western Europe and the final opening of the Atlantic Ocean during the Mesozoic.

Acknowledgments We acknowledge Alfredo Fernández Larios and José González del Tánago for their assistance with the electron microprobe analyses in the CAI of Microscopía Electrónica (UCM). We also thank Rex Taylor and Tyna Hayes from the Southampton Oceanography centre, for their help in analysing samples by TIMS. The *Access to Research Infrastructure action of the Improving Human Potential Programme*, supported by the European Community, has let us carry out the laser mineral analyses at the University of Bristol, the Pb isotope analyses at the Swedish Museum of Natural History and part of the Sr–Nd isotope analyses at the National Oceanography Centre of Southampton. This work is included in the objectives of, and supported by, the CGL2004-02515 project of the Ministerio de Educación y Ciencia of Spain.

References

Alibert C (1985) A Sr–Nd isotope and REE study of late Triassic dolerites from the Pyrenees (France) and the Messejana dyke (Spain and Portugal). Earth Planet Sci Lett 73:81–90

Bea F, Montero P, Molina JF (1999) Mafic precursors, peraluminous granitoids, and late lamprophyres in the Avila batholith; a model for the generation of Variscan batholiths in Iberia. J Geol 107:399–419

Bellon H, Chauris L, Hallegouet B, Thonon P (1988) Magmatisme fissural permien et triasique dans le Pays de Léon (Massif armoricain, France). C R Géosci 307:2049–2054

Bernard-Griffiths J, Peucat JJ, Sheppard S, Vidal P (1985) Petrogenesis of Hercynian leucogranites from the southern Armorican Massif: contribution of REE and isotopic (Sr, Nd, Pb and O) geochemical data to the study of source rock characteristics and ages. Earth Planet Sci Lett 74:235–250

Bonin B (1988) From orogenic to anorogenic environments: evidence from associated magmatic episodes. Schweiz Mineral Petrogr Mitt 68:301–311

Bonin B (2004) Do coeval mafic and felsic magmas in post-collisional to within-plate regimes necessarily imply two contrasting, mantle and crustal, sources? A review. Lithos 78:1–24

Burke K, Kidd WSF, Wilson JT (1973) Relative and latitudinal motion of Atlantic hot spots. Nature 245:133–138

Campbell IH (2005) Large igneous provinces and the mantle plume hypothesis. Elements 1:265–269

Carignan J, Hild P, Mevelle G, Morel J, Yeghicheyan D (2001) Routine analyses of trace elements in geological samples using flow injection and low pressure on-line liquid chromatography coupled to ICP-MS; a study of geochemical reference materials BR, DR-N, UB-N, AN-G and GH. Geostand Newslett 25:187–198

Carraro A, Visonà D (2003) Mantle xenoliths in Triassic camptonite dykes of the Predazzo area (Dolomites, northern Italy); petrography, mineral chemistry and geothermobarometry. Eur J Mineral 15:103–115

Casillas R, Vialette Y, Peinado M, Duthou JL, Pin C (1991) Ages et caractéristiques isotopiques (Sr, Nd) des granitoides de la Sierra de Guadarrama occidentale (Espagne). Abstract Séance Spécialisée Soc. Géol. France Mém. Jean Lameyre, s/n

Chalapathi Rao NV, Gibson SA, Pyle DM, Dickin AP (2004) Petrogenesis of Proterozoic lamproites and kimberlites from the Cuddapah basin and Dharwar craton, Southern India. J Petrol 45:907–948

Cocherie A, Rossi P, Fanning CM, Guerrot C (2005) Comparative use of TIMS and SHRIMP for U–Pb zircon dating of A-type granites and mafic tholeiitic layered complexes and dykes from the Corsican Batholith (France). Lithos 82:185–219

Cortesogno L, Cassinis G, Dallagiovanna G, Gaggero L, Oggiano G, Ronchi A, Seno S, Vanossi M (1998) The Variscan post-collisional volcanism in Late Carboniferous-Permian sequences of Ligurian Alps, Sourthern Alps and Sardinia (Italy): a synthesis. Lithos 45:305–328

Debon F, Zimmermann JL (1993) Mafic dykes from some plutons of the western Pyrenean Axial Zone (France, Spain): markers of the transition from late-Hercynian to early-Alpine events. Schweiz Mineral Petrogr Mitt 73:421–433

Doblas M, Oyarzun R, López-Ruiz J, Cebriá JM, Youbi N, Mahecha V, Lago M, Pocoví A, Cabanis B (1998) Permo-Carboniferous volcanism in Europe and northwest Africa: a superplume exhaust valve in the centre of Pangaea? J African Earth Sci 26:89–99

Dostal J, Dupuy C, Carron JP, Dekerneizon ML, Maur RC (1983) Partition coefficients of trace elements: application to volcanic rocks of St Vincent, West-Indies. Geochim Cosmochim Acta 47:525–533

Dunn AM, Reynolds PH, Clarke DB, Ugidos JM (1998) A comparison of the age and composition of the Sherburne Dyke, Nova Scotia, and the Messejana Dyke, Spain. Can J Earth Sci 35:1110–1115

Eichhorn R, Loth G, Höll R, Finger F, Schermaier A, Kennedy A (2000) Multistage Variscan magmatism in the central Tauern Window (Austria) unveiled by U/Pb SHRIMP zircon data. Contrib Mineral Petrol 139:418–435

Ernst RE, Buchan KL (1997) Giant radiating dyke swarms: their use in identifying pre-Mesozoic large igneous provinces and mantle plumes. In: Mahoney JJ, Coffin MF (eds) Large igneous provinces. Continental, oceanic, and planetary flood volcanism. AGU Geophysical Monograph 100, pp 297–333

Fernández Suárez J, Arenas R, Jeffries TE, Whitehouse MJ, Villaseca C (2006) A U-Pb study of zircons from a lower crustal granulite xenolith of the Spanish Central system: a record of Iberian lithospheric evolution from the Neoproterozoic to the Triassic. J Geol 114:471–483

Fernández M, Marzán I, Correia A, Ramalho E (1998) Heat flow, heat production, and lithospheric thermal regimen in the Iberian Peninsula. Tectonophysics 291:29–53

Foley SF (1992) Petrological characterization of the source components of potassic magmas: geochemical and experimental constraints. Lithos 28:187–204

Foley SF, Venturelli G, Green DH, Toscani L (1987) The ultrapotassic rocks; characteristics, classification, and constraints for petrogenetic models. Earth-Sci Rev 24:81–134

Foley SF, Jackson SE, Fryer BJ, Greenough JD, Jenner GA (1996) Trace element partition coefficients for clinopyroxene and phlogopite in an alkaline lamprophyre from Newfoundland by LAM-ICP-MS. Geochim Cosmochim Acta 60:629–638

Franke W (1989) Variscan plate tectonics in central Europe: current ideas and open questions. Tectonophysics 169:221–228

Frey FA, Green DH, Roy SD (1978) Integrated models of basalt petrogenesis: a study of quartz tholeiites to olivine melilitites from south eastern Australia utilizing geochemical and experimental petrological data. J Petrol 19:463–513

Galindo C, Huertas MJ, Casquet C (1994) Cronología Rb-Sr y K-Ar de diques de la Sierra de Guadarrama (Sistema Central Español). Geogaceta 16:23–26

Gardien V, Paquette JL (2004) Ion microprobe and ID-TIMS U-Pb dating on zincon grains from leg 173 amphibolites: evidence for Permian magmatism on the West Iberian margin. Terra Nova 16:226–231

Govindaraju K (1994) Compilation of working values and sample description for 383 geostandards. Geostand Newslett 18:1–158

Green TH (1995) Significance of Nb/Ta as an indicator of geochemical processes in the crust-mantle system. Chem Geol 120:347–359

Gutiérrez Marco JC, San José MA, Pieren AP (1990) Central-Iberian Zone. Post-Cambrian Paleozoic stratigraphy. In: Dallmeyer RD, Martínez García E (eds) Pre-Mesozoic geology of Iberia. Springer, Berlín, pp 160–171

Hart SR, Dunn T (1993) Experimental cpx/melt partitioning of 24 trace elements. Contrib Mineral Petrol 113:1–8

Hawkesworth CJ, Kempton PD, Rogers NW, Ellam RM, van Calsteren PW (1990) Continental mantle lithosphere, and shallow level enrichment processes in the earth's mantle. Earth Planet Sci Lett 96:256–268

Heeremans M, Faleide JI, Larsen BT (2004) Late Carboniferous-Permian of NW Europe: an introduction to a new regional map. In: Wilson M, Neumann ER, Davies GR, Timmerman MJ, Heeremans M, Larsen B (eds) Permo-Carboniferous magmatism and rifting in Europe. Geol Soc London Spec Publ, vol 223, London, pp 75–88

Ionov DA, Griffin WL, O'Reilly SY (1997) Volatile-bearing minerals and lithophile trace elements in the upper mantle. Chem Geol 141:153–184

Irving AJ, Frey FA (1984) Trace element abundances in megacrysts and their host basalts; constraints on partition coefficients and megacryst genesis. Geochim Cosmochim Acta 48:1201–1221

Irving E (1977) Drift of the major continental blocks since the Devonian. Nature 270:304–309

Kirstein LA, Dunai T, Davies G, Upton BJ, Nikogosian IK (2004) Evidence of heterogeneous mantle beneath Scotland during the Permo-Carboniferous from helium isotopes. In: Wilson M, Neumann ER, Davies GR, Timmerman MJ, Heeremans M, Larsen B (eds) Permo-Carboniferous magmatism and rifting in Europe. Geol Soc London Spec Publ, vol 223, London, pp 243–258

Kirstein LA, Davies GR, Heeremans M (2006) The petrogenesis of Carboniferous-Permian dyke and sill intrusions across northern Europe. Contrib Mineral Petrol 152:721–742

Lago M, Arranz E, Pocoví A, Galé C, Gil-Imaz A (2004) Permian magmatism and basin dynamics in the southern Pyrenees: a record of the transition from late Variscan transtension to early Alpine extension. In: Wilson M, Neumann ER, Davies GR, Timmerman MJ, Heeremans M, Larsen B (eds) Permo-Carboniferous magmatism and rifting in Europe. Geol Soc London Spec Publ, vol 223, London, pp 439–464

Lago M, Gil A, Arranz E, Galé C, Pocoví A (2005) Magmatism in the intracratonic Central Iberian basins during the Permian: Palaeoenvironmental consequences. Palaeo 229:83–103

LaTourrette T, Hervig RL, Holloway JR (1995) Trace element partitioning between amphibole, phlogopite, and basanite melt. Earth Planet Sci Lett 135:13–30

Leake BE, Woolley AR, Arps CES, Birch WD, Gilbert MC, Grice JD, Hawthorne FC, Kato A, Kisch HJ, Krivovichev VG, Linthout K, Laird J, Mandarino JA, Maresch WV, Nickel EH, Rock NMS, Schumacher JC, Smith DC, Stephenson NCN, Ungaretti L, Whittaker EJW, Youzhi G (1997) Nomenclature of amphiboles; report of the subcommittee on amphiboles of the International Mineralogical Association, Commission on New Minerals and Mineral Names. Can Mineral 35:219–246

Le Bas MJ, Le Maitre RW, Streckeisen A, Zanettin B (1986) A chemical classification of volcanic rocks based on the total alkali-silica diagram. J Petrol 27:745–750

Le Maitre RW, Streckeisen A, Zanettin B, Le Bas MJ, Bonin B, Bateman P, Bellieni G, Dudek A, Efremova S, Keller J, Lameyre J, Sabine PA, Schmid R, Sorensen H, Woolley AR (2002) Igneous rocks: a classification and glossary of terms. Cambridge University Press, Cambridge, pp 236

Matsui Y, Onuma N, Nagasawa H, Higuchi H, Banno S (1977) Crystal structure control in trace element partition between crystal and magma. Tectonics 100:315–324

McDonough WF, Sun SS (1995) The composition of the Earth. Chem Geol 120:223–253

McHone JG (2000) Non-plume magmatism and rifting during the opening of the central Atlantic Ocean. Tectonophysics 316:287–296

McKenzie D (1989) Some remarks on the movement of small melt fractions in the mantle. Earth Planet Sci Lett 95:53–72

McKenzie D, O'Nions RK (1991) Partial melt distributions from inversion of rare earth element concentrations. J Petrol 32:1021–1091

Monaghan AA, Pringle MS (2004) $^{40}Ar/^{39}Ar$ geochronology of Carboniferous-Permian volcanism in the Midland Valley, Scotland. In: Wilson M, Neumann ER, Davies GR, Timmerman MJ, Heeremans M, Larsen B (eds) Permo-Carboniferous magmatism and rifting in Europe. Geol Soc London Spec Publ, vol 223, London, pp 219–241

Monjoie P (2004) The Mont Collon mafic complex (Austroalpine Dent Blanche nappe). Doctoral Thesis, University of Lausanne, pp 163

Morimoto N, Fabries J, Ferguson AK, Ginzburg IV, Ross M, Seifert FA, Zussman J, Aoki K, Gottardi G (1988) Nomenclature of pyroxenes. Am Mineral 73:1123–1133

Muttoni G, Kent DV, Garzanti E, Brack P, Abrahamsen N, Gaetani M (2003) Early Permian Pangea 'B' to Late Permian Pangea 'A'. Earth Planet Sci Lett 215:379–394

Navon O, Stolper E (1987) Geochemical consequences of melt percolation; the upper mantle as a chromatographic column. J Geol 95:285–307

Neumann ER, Wilson M, Heeremans M, Spencer EA, Obst K, Timmerman MJ, Kirstein L (2004) Carboniferous–Permian rifting and magmatism in southern Scandinavia, the North Sea and northern Germany: a review. In: Wilson M, Neumann ER, Davies GR, Timmerman MJ, Heeremans M, Larsen B (eds) Permo-Carboniferous magmatism and rifting in Europe. Geol Soc London Spec Publ, vol 223, London, pp 11–40

Nickel KG (1986) Phase equilibria in the system SiO_2–MgO–Al_2O_3–CaO–Cr_2O_3 (SMACCr) and their bearing on spinel/garnet lherzolite relationships. Neues Jahrb Mineral Abh 155:259–287

Obst K, Solyom Z, Johansson L (2004) Permo-Carboniferous extension-related magmatism at the SW margin of the Fennoscandian Shield. In: Wilson M, Neumann ER, Davies GR,

Timmerman MJ, Heeremans M, Larsen B (eds) Permo-Carboniferous magmatism and rifting in Europe. Geol Soc London Spec Publ, vol 223, London, pp 259–288

Orejana D, Villaseca C (2008) Heterogeneous metasomatism in cumulate xenoliths from the Spanish Central System: implications on percolative fractional crystallization of lamprophyric melts. In: Coltorti M, Gregoire M (eds) Metasomatism in oceanic and continental lithospheric mantle. Geol Soc London Spec Publ, vol 293, London, pp 101–120

Orejana D, Villaseca C, Billström K (2005) A PREMA asthenospheric component for the Permian alkaline dykes of the Spanish Central System. Geochim Cosmochim Acta 69(Supp 1):A855

Orejana D, Villaseca C, Paterson BA (2006) Geochemistry of pyroxenitic and hornblenditic xenoliths in alkaline lamprophyres from the Spanish Central System. Lithos 86:167–196

Orejana D, Villaseca C, Paterson BA (2007) Geochemistry of mafic phenocrysts from alkaline lamprophyres of the Spanish Central System: implications on crystal fractionation, magma mixing and xenoliths entrapment within deep magma chambers. Eur J Mineral 19:817–832

Oyarzun R, Doblas M, López-Ruiz J, Cebriá JM (1997) Opening of the central Atlantic and asymmetric mantle upwelling phenomena: implications for long-lived magmatism in western North Africa and Europe. Geology 25:727–730

Peacock SM (1990) Fluid processes in subduction zones. Science 248:329–337

Perini G, Cebriá JM, López-Ruiz JM, Doblas M (2004) Permo-Carboniferous magmatism in the variscan belt of Spain and France: implications on mantle sources. In: Wilson M, Neumann ER, Davies GR, Timmerman MJ, Heeremans M, Larsen B (eds) Permo-Carboniferous magmatism and rifting in Europe. Geol Soc London Spec Publ, vol 223, London, pp 415–438

Portugal-Ferreira M, Macedo CR (1977) Actividade basaltica Permico-Liassica no territorio portugues; uma achega para a datacao. Permo-Liassic basaltic activity in Portugal; preliminary dating. Mem Not Publ Museo Lab Min Geol Univ Coimbra 83:39–52

Ringwood AE (1970) Petrogenesis of Apollo 11 basalts and implications for lunar origin. J Geoph Res 75:6453–6479

Rock NMS (1991) Lamprophyres. Blackie, Glasgow, pp 285

Rottura A, Bargossi GM, Caggianelli A, Del Moro A, Visona D, Tranne CA (1998) Origin and significance of the Permian high-K calc-alkaline magmatism in the central-eastern Southern Alps, Italy. Lithos 45:329–348

Rudnick RL, Gao S (2003) Composition of the continental crust. In: Holland HD, Turekian KK (eds) Treatise on Geochemistry 3. The crust. Elsevier, Pergamon, Oxford, pp 1–64

Scarrow JH, Bea F, Montero P, Molina JF, Vaughan APM (2006) A precise late Permian $^{40}Ar/^{39}Ar$ age for Central Iberian camptonitic lamprophyres. Geol Acta 4:451–459

Stemmerik L, Ineson JR, Mitchell JG (2000) Stratigraphy of the Rotliegend Group in the Danish part of the northern Permian Basin, North Sea. J Geol Soc Lond 157:1127–1136

Sun SS, McDonough WF (1989) Chemical and isotopic systematics of oceanic basalts; implications for mantle composition and processes. In: Saunders AD, Norrey MJ (eds) Magmatism in ocean basins. Blackwell, Geol Soc Spec Publ, vol 42, Oxford, pp 313–345

Taura H, Yurimoto H, Kurita K, Sueno S (1998) Pressure dependence on partition coefficients for trace elements between olivine and the coexisting melts. Phys Chem Earth 25:469–484

Tejero R, Ruiz J (2002) Thermal and mechanical structure of the central Iberian Peninsula lithosphere. Tectonophysics 350:49–62

Tiepolo M, Vannucci R, Oberti R, Foley SF, Bottazzi P, Zanetti A (2000) Nb and Ta incorporation and fractionation in titanian pargasite and kaersutite: crystal–chemical constraints and implications for natural systems. Earth Planet Sci Lett 176:185–201

Traversa G, Ronca S, Del Moro A, Pasquali C, Buraglini N, Barabino G (2003) Late to post-Hercynian dyke activity in the Sardinia-Corsica domain: a transition from orogenic calc-alkaline to anorogenic alkaline magmatism. Boll Soc Geol It Vol Spec 2:131–152

Ubanell AG (1981) Significado tectónico de los principales sistemas de diques en un sector del Sistema Central Español. Cuad Geol Iber 7:607–622

Upton BGJ, Stephenson D, Smedley PM, Wallis SM, Fitton JG (2004) Carboniferous and Permian magmatism in Scotland. In: Wilson M, Neumann ER, Davies GR, Timmerman MJ, Heeremans M, Larsen B (eds) Permo-Carboniferous magmatism and rifting in Europe. Geol Soc London Spec Publ, vol 223, London, pp 195–218

Villaseca C, Herreros V (2000) A sustained felsic magmatic system: the Hercynian granitic batholith of the Spanish Central System. Edinburgh Geol Soc Trans Earth Sci 91:207–219

Villaseca C, Barbero L, Reyes J, Santos Zalduegui JF (1998a) Nuevos datos petrológicos, geocronología (Rb–Sr) y geoquímica isotópica (Sr, Nd) del plutón de Ventosilla (Sierra de Guadarrama, Sistema Central Español). Geogaceta 23:169–172

Villaseca C, Barbero L, Rogers G (1998b) Crustal origin of Hercynian peraluminous granitic batholiths of central Spain: petrological, geochemical and isotopic (Sr, Nd) arguments. Lithos 43:55–79

Villaseca C, Downes H, Pin C, Barbero L (1999) Nature and composition of the lower continental crust in central Spain and the granulite–granite linkage: inferences from granulitic xenoliths. J Petrol 40:1465–1496

Villaseca C, Orejana D, Pin C, López García JA, Andonaegui P (2004) Le magmatisme basique hercynien et post-hercynien du Système Central Espagnol: essai de caractèrisation des sources manteliques. C R Géosci 336:877–888

White R, McKenzie D (1989) Magmatism at rift zones: the generation of volcanic continental margins and flood basalts. J Geoph Res 94:7685–7729

Wilson M (1989) Igneous petrogenesis: a global tectonic approach. Unwin Hyman, Boston, pp 466

Wilson M (1997) Thermal evolution of the central Atlantic passive margins: continental break-up above a Mesozoic super-plume. J Geol Soc Lond 154:491–495

Wilson M, Neumann ER, Davies GR, Timmerman MJ, Heeremans M, Larsen BT (2004) Permo-Carboniferous magmatism and rifting in Europe. Geol Soc London Spec Publ, vol 223, London, pp 498

Zanetti A, Tiepolo M, Oberti R, Vannucci R (2004) Trace-element partitioning in olivine: modelling of a complete data set from a synthetic hydrous basanite melt. Lithos 75:39–54

Zeck HP, Wingate MTD, Pooley G (2007) Ion microprobe U–Pb zircon geochronology of a late tectonic granitic–gabbroic rock complex within the Hercynian Iberian belt. Geol Mag 144:157–177

Ziegler PA (1993) Late Palaeozoic-Early Mesozoic plate reorganization: evolution and demise of the Variscan fold belt. In: Von Raumer JF, Neubauer F (eds) Pre-Mesozoic geology in the Alps. Springer, Berlin, pp 203–216

Ziegler PA, Schumacher ME, Dézes P, vam Wees J-D, Cloetingh S (2004) Post-Variscan evolution of the lithosphere in the Rhine Graben area: constraints from subsidence modelling. In: Wilson M, Neumann ER, Davies GR, Timmerman MJ, Heeremans M, Larsen BT (eds) Permo-Carboniferous magmatism and rifting in Europe. Geol Soc London Spec Publ, vol 223, London, pp 289–317

Zindler A, Hart SR (1986) Chemical geodynamics. Ann Rev Earth Planet Sci 14:493–571